Transformation of dense shelf water cascade into turbidity currents: insights from high-resolution geophysical datasets

Nan Wu[1*], Guangfa Zhong[1], Yakufu Niyazi[2], Harya D. Nugraha[3], Michael J. Steventon[4]

[1]State Key Laboratory of Marine Geology, Tongji University, 1239 Siping Road, Shanghai, 200092, China

[2]Minderoo-UWA Deep-Sea Research Centre, School of Biological Sciences and UWA Oceans Institute, The University of Western Australia, Perth, WA 6009, Australia

[3]Center for Sustainable Geoscience, Universitas Pertamina, Jakarta, 12220, Indonesia

[4]Shell Research, Shell Centre, London, SE1 7NA, UK

[*]Email: nanwu@tongji.edu.cn

ABSTRACT

Dense shelf water cascade (DSWC) is a common oceanographic phenomenon on many continental shelves. Previous studies indicate that the DSWC could shape seabed physiography and carry seawater, sediment, and organic carbon a long distance from the continental shelf to the basin floor. However, it remains enigmatic how these DSWC's interact with seabed geomorphology and travel long distances from the shallow to deep marine environments. In this study, we employed high-resolution multibeam bathymetry, 2D and 3D seismic reflection, core description, sediment grain size data from the Gippsland Basin, southeast offshore Australia. The continental shelf of the central Gippsland Basin stores sediment supplied by the along-shelf transported DSWC. Seismic reflection data reveal that cyclic steps are common on the shelf and slope, indicating a downslope-transported, supercritical current-dominated environment. Core observation and grain size analyses reveal that coarse-grained, Ta-typed turbidites are the major facies, indicating the presence of high-intensity downslope-traversing turbidity currents. Thus, supercritical turbidity currents are the dominant sedimentary process in the central Gippsland Basin. We illuminate that DSWC can interact with pre-existing submarine landslides, resuspending sediment and igniting downslope-transported turbidity currents. Upon ignition, the turbidity current can evolve into a supercritical regime, leaving complex seabed geomorphology and allowing shallow water to travel across the shelf and extend more than 80 km down the lower slope. We imply that the transformation of DSWC into turbidity currents is a new machinism for the inition of turbidity currents. As revealed by our literature analysis, this process should be common on outer continental shelves globally. As the strength, frequency, and pathway of DSWC are sensitive to seawater temperature variations dictated by climate change, we therefore infer that this current transformation process has critical implications for predicting how seabed geomorphology, sedimentation, and geohazards respond to changing oceanographic and climate conditions.

Keywords: Dense shelf water cascade (DSWC), Current transformation, Turbidity-current initiation, Gippsland Basin

INTRODUCTION

Along the continental shelves, seasonal evaporation during summer and cooling during winter can generate a cross-shelf density gradient that drives denser seawater transport seawards along the seabed (Ivanov et al., 2004; Canals et al., 2006). This process is defined as dense shelf water cascade (hereafter DSWC). The DSWC is a climate-driven oceanographic phenomenon prominent throughout the tropical to the high-latitude continental margins (Figure 1A; Ivanov et al., 2004; Amblas and Dowdeswell, 2018; Mahjabin et al., 2020; Gales et al., 2021). The DSWC has been repeatedly measured by both long-term and high-frequency in situ measurements (i.e. Conductivity-Temperature-Depth measures; CTDs), and has been well studied by physical oceanography observations (i.e. Canals et al., 2006; Puig et al., 2008; Canals et al., 2009). Once the DSWC is initiated, it sinks and overflows the shelf area under the influence of gravity, cascading downslope until it reaches its density equilibrium depth (also known as neutral density level; Figure 1B) (Fohrmann et al., 1998; Canals et al., 2009). Results indicate the DSWC can travel more than 10,000 km along the coastline and descends more than 1000 m down the slope and eventually flooding the basin floor (Figure 1B; Ivanov et al., 2004; Canals et al., 2009; Mahjabin et al., 2020). When transported along the shelf, DSWC can travel at a high speed (i.e. 1.2 m/s) and is highly erosive (Canals et al., 2006; Puig, 2017). For example, the DSWC can dislodge an c. 400 kg anchor at least 3 km away from its mooring position, polish rusty iron of the train wheel very shiny through continuous sandblasting assocaited with the powerful cascading currents (Puig et al., 2008).

The DSWC can affect a large portion of the seabed, induce erosion and deposition, and generate bottom nepheloid layers (zones) that contain significant amounts of suspended sediments and subsequently produce fast travelling gravity flows (Figure 1B; Canals et al., 2006; Puig, 2017). At specific locations, canyons are often the major conduits and determine the paths and spreading conditions for the DSWC (Canals et al., 2006; Morrison et al., 2020; Gales et al., 2021). The DSWC has proved to be an effective seabed-sculpting agent and is capable of large amounts of water and heat, sediments, organic carbon, marine pollutants and nutrients transfer from shallow marine to the deep ocean (Canals et al., 2006; Puig et al., 2008; Canals et al., 2009). Therefore, the DSWC plays an important role in global deep-ocean circulation, sediment source-to-sink, earth's climate system, carbon and biogeochemical cycles (Amblas and Dowdeswell, 2018).

Despite the extensive existing literature, some important questions remain to be addressed. Firstly, the process of how DSWC produces gravity flows and shape seabed geomorphology is still poorly understood (Canals et al., 2006; Talling, 2014). Secondly, the reasons for the DSWC spreading over a considerable distance across the shelf and even reaching the lower slope remain unclear. Here we attempt to unravel these important, yet under-explored aspects of DSWC, by presenting observations based on high-resolution bathymetric multibeam, seismic reflection, piston core and sediment grain size datasets from the offshore Gippsland Basin, Australia. The occurrence of the DSWC has brought large amount of sediment and resulted in extremely complex seabed geomorphology in the central Gippsland Basin (Godfrey et al., 1980; Tomczak, 1985; Mitchell et al., 2007b). The complex seabed geomorphology reflects the action of a range of oceanographic and sedimentary processes at multiple spatiotemporal scales. Therefore, the central region of the Gippsland Basin provides an ideal place to investigate the remaining questions we raised above. We revealed that the DSWC can interact with pre-existing seabed depressions caused by submarine landslides, igniting turbidity currents and leaving erosional bedforms on the seabed. We highlight that the transformation of the DSWC into turbidity currents is a new sedimentary process and should be common on many continental shelves globally. The transition from the DSWC to the turbidity current is crucial to understanding the evolution of seabed geomorphology through time, as well as the mechanisms that account for the long-distance transportation of the DSWC under the influence of dynamic climate and oceanographic processes.

GEOLOGICAL SETTING

The Gippsland Basin

The offshore Gippsland Basin is dominated by a cool-water carbonate system located on SE Australia's passive margin, between the mainland of Australia and Tasmania (Figures 2A, 2B; Rahmanian et al., 1990). It is one of Australia's most prolific hydrocarbon provinces, fisheries, and potential carbon storage, and holds a number of other potential marine resource applications (Rahmanian et al., 1990; Mitchell et al., 2007a; Mitchell et al., 2007b). The Gippsland Basin belongs to a series of rift basins formed along the southern margin of the Australian plate, due to the separation of

Antarctica and Australian continents during the breakup of Gondwana in the Mesozoic (Colwell et al., 1993). Since the Pleistocene, the Gippsland Basin has been detached from major river sources, allowing the development of a cool water carbonate province with minimal terrigenous input (Mitchell et al., 2007b). The margin of the Gippsland Basin is dominated by a c. 100 km wide embayment, and the SE margin of the basin is floored by c. 120 km long and 15-70 km wide, ESE-trending Bass Canyon system (Figures 2A, 2B). The Bass Canyon is one of the world's largest submarine canyons and constitutes the SE boundary of the Gippsland Basin (Mitchell et al., 2007b). The Bass Canyon has acted as a major conduit and key element in the source-to-sink system in the SE Australian area since the Late Cretaceous (approximately 80Ma; Hill et al., 1998). At present, it still transfers sediments, oxygen, nutrient, pollutants, and organic matter from the canyon head to the Tasman Abyssal Plain at almost 4500 m water depth (Figure 2B).

Climate and oceanography

The Bass Strait is a shallow (water depth range from 40-60 m) coastal sea between mainland Australia and Tasmania, connecting the Great Australian Bight in the west and the Tasman Sea in the east (Figure 2A; Tomczak, 1985; Lavering, 1994). In winter, the shallow Bass Strait imposes a limit on the penetration of thermal convection, and as a consequence, Bass Strait seawater cools rapidly and has a higher salinity than those of the surface layer in the Tasman Sea (Lavering, 1994). Therefore, when seawater leaves the Bass Strait on its eastern side, it has a prominent density contrast against the Tasman Sea water (Tomczak, 1985). As a consequence, cold, denser Bass Strait seawater can flow into and sink beneath the warmer, fresher water of the Gippsland shelf, generating the northeast flowing Bass Cascade Current (hereafter BCC) which sinks to the 200-400 m isobaths and extends more than tens of kilometres (Figure 2B; Godfrey et al., 1980; Li et al., 2005; Mitchell et al., 2007b). Observations from the ocean bottom stations have revealed that the BCC is the densest seawater offshore SE Australia, it is active every year and is with an average transport rate of 1.0 Sverdrups (Sv; $1Sv=10^6 m^3/s$) (Middleton and Bye, 2007). The transportation of the BCC has transported significant quantities of water and sediments and spreads along the shelf edge over a long distance (Boland, 1971). For example, distinctive temperature-salinity anomalies are found at 200-800 m depth in Tasman Sea, most likely caused by Bass Strait seawater penetration (Figure 2C; Boland, 1971). In the Gippsland Basin, the central continental shelf is dominated by the Westerly wind throughout the year (especially in winter; Figure 2B; Li et al., 2005). The eastward-flowing Westerly wind flows at 10-30 km/h with maximum gusts reaching 100 km/h. Therefore, the Westerly wind has created a moderate to high energy wave-dominated environment and a robust NE-transported Ekman Transport Flow (ETF) in a water depth of c. 200-300 m (Figure 2B; Mitchell et al., 2007a; O'Brien et al., 2018). The East Australia Current (EAC) is a western boundary current that carries warm equatorial waters and flows southward adjacent to the Australia's southeast coast (Figure 2B, 2D). It is up to 500 m deep and 100 km wide, occasionally extending far enough south to reverse the movement of water in the Gippsland Basin during summer months (Li et al., 2005).

Therefore, the combination of seasonal northward flowing BCC, the southward flowing EAC, and northeast flowing ETF have jointly controlled the oceanography and sedimentation along SE Australia continental margin.

DATASET AND METHODOLOGY

The datasets available for this study include multibeam bathymetry data with a coverage area of c. 250,000 km^2, 2D and 3D seismic reflection data with a coverage area of c. 1700 km^2, with lithology control provided by six-piston core samples (Figures 2B, 3A).

Multibeam bathymetry

Multibeam bathymetry data for this study is sourced and can be downloaded from Geoscience Australia's Marine data portal (http://marine.ga.gov.au). The dataset is compiled from multiple bathymetric surveys and gridded at 50x50 m; hence, geomorphological features smaller than 50 m across cannot be differentiated. The multibeam bathymetry dataset covers the Gippsland Basin continental shelf, at around 200 m water depth, to the Tasman Sea Abyssal plain, at over 4000 m water depth (Figure 3A).

Seismic data

We adopt two types of seismic reflection data provided by Geoscience Australia (http://www.ga.gov.au/nopims): (i) 2D regional seismic section which is up to c. 90 km long, therefore providing excellent coverage from Gippsland Basin shelf region to Bass Canyon abyssal plain (Figure 3C); and (ii) two 3D seismic reflection surveys (Elver 3D and Tuskfish 3D), which covered an area of c. 650 km^2 and 1050 km^2, respectively (Figure 2B). Both 3D seismic datasets are zero-phase processed, and a downward decrease and increase in acoustic impedance are expressed as blue (negative) and red (positive) seismic reflections, respectively. The 3D seismic surveys have a dominant frequency content of 70 hertz and an average seismic velocity of 1700 m/s near the seabed sediment, which gives an approximate vertical resolution of c. 6 m for the near seabed sediments. The 3D seismic resolution is therefore sufficient to map the geometry of detailed seabed sedimentary and structural features. We further extract the dip illumination seismic attribute (see Appendix S1 for an explanation), from the 3D seismic dataset to determine the seabed geometries and geomorphology of the interpreted submarine deposits.

Piston Core and grain Size

Comprehensive sediment sampling and piston cores collection was conducted from RV Franklin cruise in 1998 (FR11/98) (Exon et al., 2002). In this study, we adopted six-piston cores in the continental shelf and slope areas over a water depth range of 200-2500 m. The detailed core descriptions and interpretations are compiled from (Mitchell et al., 2007b), which have provided lithological and sedimentary facies constraints for the study area. In addition, we analyzed seabed grain size distribution data from 13 locations, obtained from Geoscience Australia Marine Sediment

Database (https://portal.ga.gov.au). For the purpose of this current research, we analyzed the proportion of mud (<65 µm), sand (between 65 µm and 2 mm) and gravel (> 2mm) within each sampling locations.

RESULT

We divide the Gippsland Basin into Northern, Central, and Southern regions based on geographical position and seabed morphology (Figure 3A, 3B). The continental shelf of the Central region extends seaward for approximately 70 km with an average dip of 0.8^o then abruptly steepens to 8.8^o in the slope (Figure 3C). The water depth of the Central region ranges from 0-500 m on the shelf and from 500-2000 m on the slope (Figure 3A). Below we describe the seabed geomorphology and the major sedimentary environments from the shelf to the slope in the Central region of the Gippsland Basin.

Seabed geomorphology of the shelf area

Observation: The Central region is characterized by an erosional seabed (Figure 4A, 4B). On the shelf, a set of north-trending scallop-shaped scarps have been observed near the outer shelf area (Figure 4C). Seismic sections indicate the scallop-shaped scarps show a clear truncation edge and erosional base surface (termed as basal shear surface), marking the boundary that differentiates the overlying undeformed strata from the deformed sediments (Figures 5A). Downslope (eastward) to the scarps, a series of sediment wave fields have been observed along the middle part of the outer shelf (Figure 4B, 4C). Further downslope, the sediment waves are dissected by a set of irregular discontinuous concave-downslope scours occur at the southwestern part of the shelf (Figures 4B, 4C). In the seismic section, the scours are ranging from 1.2-1.7 km in width, 1.7-3.4 km in length (spacing), from 80-200 m in depth, and with aspect ratio (wavelength/height) from 167-221 (Figure 5B). These scours are normally characterized by truncated, steep lee sides and gentle, slightly upslope-dipping stoss sides (Figure 5B). Buried scours are observed beneath their seabed counterparts (Figure 5B). The buried scours contain sub-parallel, relatively high-amplitude seismic reflections, and show upslope migration by erosion in the lee side and deposition in the stoss side (Figure 5B).

Further NE, three sets of scours aligned in distinctive or discontinuous channel-shaped depressions have been observed in the centre part of the shelf (Figure 4C). The crests of these scours are consistently oriented approximately north-south, being confined in the axis of channel-shaped morphology (Figure 4C). Seismic sections cutting along the thalweg of the channel-shaped depressions show a series of bedforms that form a train of steps and stretch over a distance of 10-16 km (Figures 5C, 5D). These bedforms range from 0.2-0.7 km in width, 0.9-1.2 km in wave length, 20-60 m in wave height, and with aspect ratio from 46-167 (Figures 5C, 5D). A single bedform is characterized by a steep scarp indicated by truncated seismic reflections that form the lee side contrast with a gently, lower relief slope at the stoss side (Figures 5C, 5D).

Further NE of the shelf, at least two well-developed channels have been observed in the eastern part of the shelf (Figure 4C). Nevertheless, these channels only extend to the shelf break, and no clear erosions have been observed within the slope (Figures 4B, 4C). These channels vary from 2–10 km in width, and 100–325 m in depth (Figure 4B). They initially trend SSE and then sharply divert to the NE within a few kilometres distance across the shelf break, and ultimately run to the slope after passing through the shelf break (Figures 4B, 4C). A set of longitudinal lineations have been observed on the southern flank of the channels (Figure 4C). These lineations are c. 8 km long, they are evenly spaced and predominantly oriented parallel to the channel axis. In the seismic section, the longitudinal lineations show a stair-shaped cross-sectional geometry and truncations (Figure 5E).

Interpretation: The scalloped scarps developed near the outer shelf indicate a gradual broadening over time is likely caused by slope failures (i.e. Lee and Chough, 2001). The scalloped scarps are thus interpreted as headwall scarps associated with a buried landslide (Figure 5A). The scours, scour trains and channels are developed above the landslide’s basal shear surface, suggesting the landslide predate these bedforms (Figures 5B-E). The sediment wave fields developed within the scarps is evident for the presence of downslope currents (i.e. Fildani et al., 2006). The asymmetrical cross-sectional geometry, large aspect ratio, upslope migration trend indicate the scours are cyclic steps (also interpreted as cyclic scours) that is carved by downslope flowing currents through the force of hydraulic jumps (Figrue 5B; Fildani et al., 2006; Kostic, 2011). The buried scours are interpreted as partially depositional cyclic steps, formed when sediment erosion on the lee side is less than sediment deposition on the stoss side (Slootman and Cartigny, 2020). The presence of the partially depositional cyclic steps suggests that the downslope flowing currents were active in the Central region for an extended period of time. The scours that aligned in the channel template is interpreted as trains of erosional cyclic steps (i.e. Taki and Parker, 2005; Fildani et al., 2013; Zhong et al., 2015). The erosional cyclic step trains can represent the incipient channel formation (i.e. Fildani et al., 2006; Fildani et al., 2013).

The channel's diversion near the shelf edge could be resulted from the Westerly wind-induced Ekman transport flow (ETF). Due to the influence of the Coriolis effect, the ETF follows a NE-NNE direction, which interacts with the sedimentary systems along the edge of the continental shelf (Mitchell et al., 2007a). Therefore, the ETF transportation may have influenced the sediments distribution near the shelf edge and contributed to the channel axis deviation. The EAC is less likely contribute to the deviation of the channel axis, as it separates from the coast approximately between 30°S and 32°S, splitting into eddy-dominated southern and eastern extensions (Cetina-Heredia et al., 2014; Oke et al., 2019). The major eddies are anticlockwise, and therefore, the channel courses should be diverted to the southeast direction, which is opposite to our observation.

The longitudinal lineations developed within the channels are interpreted as sedimentary furrows similar to those observed in other submarine settings (i.e. Wynn and Stow, 2002; Puig et al., 2008). Studies of furrows show that these features were formed due to recurring, stable, and directional currents (i.e. turbidity currents) erosion through time (e.g. Flood, 1983; Puig et al., 2008). The presence of furrows in this study suggests that the ambient downslope flowing currents may have strong and persistent energy, carrying coarse particles that erode the canyon sidewall, generating furrows (Flood, 1983). The sole appearance of furrows on the channel's southern flank suggests that the downslope flowing currents preferential arrival across the southern channel flank.

Seabed geomorphology of the slope area

Observation: Near the upper slope, gullies and landslide scarps are widely distributed on the slope between water depths 700 to 2000 m (Figure 6). The gullies extend several kilometres from the upper slope to the lower slope, terminating as the slope angle decrease and intersects with the Bass Canyon head (Figures 4B, 6). The gullies are straight and oriented to the dip direction of the slope, characterized by linear morphology, rounded heads and narrow bodies in plain view (Figure 6). Small failures and slide scarps are evident within or around the edges of the gullies. In the seismic section, these gullies are V-shaped, and have a relatively flat base reflection with clear erosive truncation along the sidewalls (Figure 7A). The gully sidewalls have a relief (incision depth) of 110-230 m, and a width of 120-280 m (Figure 7A). The landslide scarps roughly dip from NNE to SSW, with widths ranging from c. 4 km to 7km (Figure 6). In seismic sections, these scarps show a stair-shape, backward (i.e. landward) dipping geometry (Figure 7B).

Near the lower slope, scours that are aligned in train and parallel to the slope dip direction have been observed within the gullies and on the inter-gully ridges (Figure 6). Seismic sections cutting along the thalweg of the scour trains show that they are characterized by steep and erosional lee sides and gentle stoss sides, similar to the cyclic steps developed on the shelf (Figures 7B-D). These scours are 0.5-1.3 km in wavelength, 9-19 m in wave height, and aspect ratio is from 12-40. They are best developed near the lower slope, where the slope gradient drops from 9^{o}-12^{o} (near the upper slope) to 4^{o}-7^{o} (to the lower slope; Figures 7B-D). Further lower slope, giant landslide scarps that distribute more than 30 km horizontally are observed near the lowermost of the slope (Figure 6). In the seismic section, the scarps show clear truncations that separate the undeformed seabed (upslope) from the deformed erosional seabed (downslope) (Figures 7B-D).

Interpretation: Near the upper slope, the step-shaped pattern of the scarps suggests a retrogressive failure mechanism of the landslides (Figure 7B; Wu et al., 2021). As the landslides are located along the shelf edge, where cyclic wave loading can constantly rework seabed sediments. This process may account for a potential trigger mechanism leading to slope failure (i.e. Marshall et al., 1978; Bea et al., 1983). The gullies clearly incise into the landslides, suggesting that they post-date the slope failures (Figure 6). The linear gullies are interpreted as the conduits for gravity flows to transport sediment to deeper waters (Micallef and Mountjoy, 2011; Lonergan et al., 2013). The V-shaped head geometry indicates the origin of the gullies is associated with downslope gravity-driven currents (i.e. debris flow and turbidity current; Farre et al., 1983; Gales et al., 2012). Successive small failures are exhibited on the gully ridges, which is indicative of a gradual widening of the gullies (Post et al., 2022). The scour trains developed within the gullies and on the inter-gully ridges are interpreted as cyclic steps, similar to their counterparts developed on the shelf (i.e. Fildani et al., 2006). The presence of cyclic steps suggests that the slope area is also a supercritical flow regime-dominated environment, and the erosion by supercritical currents might play a role in the gully's initiation and evolution (i.e. Noormets et al., 2009; Gales et al., 2012).

Theoretically, a steeper slope generates a faster flow that is more likely to be Froude-supercritical (i.e. Fildani et al., 2006). However, it contrasts with our observations as cyclic steps are scarce on the upper slope where slope gradient is steeper (9°-12°), and are prominent on the lower slope where slope gradient is relatively gentle (4°-7°) (Figures 7B-D). This discrepancy can be explained as the higher slope gradient can cause the overflowing currents to have a faster velocity, thus suppressing their ability to decelerate and undergo internal hydraulic jumps (Kostic, 2011; Zhong et al., 2015). Due to the higher flow velocity (therefore more energetic), erosional scours and truncations are common on the upper slope (Figures 7C, 7D). Further downslope, cyclic steps preferentially form near the lower slope area (Figures 7B-D), suggesting the transition from high slope gradients to low slope gradients could promote the formation of the cyclic steps (i.e. Covault et al., 2017; Fildani et al., 2021). The construction of cyclic steps has led to the formation of local high topographies near the distal side of the lower slope (Figures 7B-D). These local topographic highs can form 12^{o}-22^{o} slopes and range from 70-130 m high, leaving a series of spatially evacuated accommodations near the distal edge of the lower slope (Figures 7B-D). These evacuated accommodations can reduce the lower slope's lateral confining pressure, thus increasing seabed instability (Bull et al., 2009). This can be evidenced by the giant submarine landslides occurring immediately adjacent to, and continuous headwall scarps developing near the distal side of the local topographic highs (Figures 7B-D). Therefore, we indicate that the local topographic highs can act as landslide-susceptible structures that ultimately prime slope failures.

Piston core and grain size analysis

Observation: Facies-1 can be observed from the shelf and slope (core #1-4 and 6; Figure 4B). On the shelf, Facies-1 are observed within the headwall scarp of buried submarine landslide (Figure 4B). Facies-1 is normally graded, moderately to well-sorted, and contains coarse-grained sand (predominately near the lower part) with a sharp top surface and an erosional base surface (Figure 8A). Facies-1 collected from the slope area suggests this facies is internally structureless and contains shelf-restricted bioclasts (core #4 and 6; Figure 4B). Facies-2 can be observed from the upper-lower slope (core #5 and 6; Figure 4B). Facies-2 contains sand- and silt-sized bioclasts, quartz and siliciclastic clay. Core observation indicates it is poorly sorted, matrix-supported and often organic-rich (Figure 8B). It also has decimetre-thick bedding with gradational contacts with bioturbation observed (Figure 8B).

There are significant differences in grain size distributions between sediment samples collected outside (west) of the landslide headwall scarps and within (east) the scarp area (Figure 8C). Sediment samples collected outside (west) of the headwall scarp show fine-to-medium grain size, and the predominant particle diameter is between 65 µm and 2 mm (Figure 8C). In comparison, sediment sample collected within the scarp exhibits sharp grain size variations (Figure 8C). Specifically, the sediment has an average particle diameter exceeding 2 mm and consists primarily of coarse-grained gravel.

Interpretation: The erosional base surface, coarse-grained, normally graded, and internally structureless nature of Facies-1 is a typical indicator of Bouma Ta-typed turbidites, which are primarily formed by down slope transported turbidity currents (Bouma, 1962). The abundance of shelf-restricted bioclasts observed from the slope suggests these turbidites originated from the shelf. Therefore, we interpret Facies-1 as turbidites formed by turbidity currents sourced from the continental shelf. The fine-grained and organic-rich nature of Facies-2 suggests it is deposited under a low energy condition. We interpret Facies-2 represents a deep marine hemipelagic environment (Mitchell et al., 2007b).

The BCC is the dominant oceanographic process on the central shelf, grain size analyses of the samples collected outside the headwall scarp show that the BCC has carry mostly fine-grained sediments (Figure 8C). The sudden change in grain size collected within the headwall scarp suggests a highly turbulent and energetic flow that is capable of carrying coarse grained sediments is active (Postma and Cartigny, 2014). Core analyses conducted in the same area indicate this highly turbulent and energetic flow is downslope transported turbidity current. Thus, the significant change in grain size may attribute to the transition from along shelf transported BCC to downslope transported turbidity current, and the transformation process occurs near the headwall scarp of submarine landslide.

DISCUSSION

Turbidity current: the dominant sedimentary process in central Gippsland Basin

The seismic interpretations reveal a continued presence of cyclic steps throughout the outer shelf and slope areas (Figures 4C and 6), which indicate a continuing role of downslope-transported supercritical currents in sculpting and remoulding the seabed in the central Gippsland Basin (i.e. Fildani et al., 2006; Kostic, 2011; Zhong et al., 2015). Published studies suggest that the overriding flow that creates cyclic steps is turbidity currents that transform from supercritical-to-subcritical flow through internal hydraulic jumps (i.e. Zhong et al., 2015; Covault et al., 2017; Fildani et al., 2021). Core observation and grain size analyses have confirmed this interpretation, as coarse-grained, Ta-typed turbidites are the major facies, indicting the presence of high-intensity downslope-traversing turbidity currents (Figures 8A, 8C; Bouma, 1962). Additionally, recent publications indicate that Ta-typed turbidites can be formed by hydraulic jump-related rapid sedimentation, often associated with high-energy supercritical turbidity currents (Figure 8A; i.e. Postma and Cartigny, 2014). Therefore, by combining the results from seismic interpretation, core observation, and grain size analyses, we interpret that turbidity currents are the dominant sedimentary process in the central Gippsland Basin.

A new process that initiates turbidity current: the transformation from the dense shelf water cascade

The origin of turbidity currents has been attributed to three main processes, transforamtion from the slope failures, hyperpycnal flows from onshore fluvial input or subglacial meltwater, and oceangraphic processes (including storms, tides, and internal waves) generated flows near the shelf edge (Piper and Normark, 2009; Talling et al., 2013). In Gippsland Basin, the Central region has been completely disconnected from onshore drainage systems since Pliocene (Mitchell et al., 2007b), and no modern submarine landslides (only buried landslide; Figure 5A) are observed in the central shelf. Additionally, the erosional features developed on the shelf is inferred to reflect a recurring, directionally stable flow that is sufficiently strong to erode the seabed. Oceangraphic processes may play a role in resuspension seabed sediments and ignite episodic flows, and their influence are often multi-directional, they lack the abality to generate recurring, directionally and stable currents. Therefore, the initiation of turbidity currents cannot be caused by either of the factors above. Hence, it is reasonable to assume that the turbidity currents in the central Gippsland Basin are caused by dense shelf water cascade currents. Below, we investigate how this current transformation process might occur.Published works indicate that the BCC propagate along and cascade across the continental shelf of the Gippsland Basin (Figures 9A, 9B; Godfrey et al., 1980; Mitchell et al., 2007b). Before flowing into the landslide-influenced area, the transportation of BCC could maintain an equilibrium condition with the bottom nepheloid layers containing significant amounts of suspended sediments (Figure 9A, 9B; Puig, 2017). If the seafloor is relatively smooth, the BCC could have kept previous conditions and continue to flow northeast. However, on the outer shelf of central Gippsland Basin, the headwall scarps of the landslide have caused local seabed depressions and slope gradient variation (Figures 9B, 9C). As the BCC moves cross and flows over these seabed depressions, the BCC can have increased shear stresses where seabed bathymetry is rough and the slope gradient is steep, thus it is capable of resuspending a significant amount of sediment (i.e. Ogston et al., 2008). Additionally, the seabed depressions can breach the equilibrium condition of the BCC, splitting the dense nepheloid layers apart (Figures 9B, 9C). Subsequently, the seabed depressions could further catch the splitted dense nepheloid layers, and force them to sink (Figure 9C). Consequently, the sinking nepheloid layers would hover the seabed and potentially accelerate in an ignitive manner when traversing the headwall scarps, generating intense sediment resuspension (Figure 9C). Accelerating flows could cause perturbations, entrain more sediment (including suspended sediments), and ultimately ignite a turbidity current (Figure 9C). The steep headwall scarps are marked by steep gradients of 7^{o}-10^{o} and are 40-70 m deep, extending over 30 km on the outer shelf (Figures 3A, 9A). The presence of the scarps could allow sediment to remain in suspension longer as the BCC moves across the shelf, resuspending unconsolidated sediments from the seabed and providing a recurrent source for turbidity current initiation (Ogston et al., 2008). Other oscillatory oceanographic processes, including Westerly winds generated strong wave actions and storms generated currents, may coincide with the BCC (or act as external forces to enhance the BCC) and jointly resuspend large amounts of seabed sediments and generate downslope flows that contribute to turbidity current initiation (Figure 9D; Micallef and Mountjoy, 2011; Talling et al., 2013).

After ignition, the steep gradient (7^{o}-10^{o}) of the headwall scarp would provide ample opportunity for turbidity currents to evolve into Froude supercritical regime and subsequently form hydraulic jumps (Figure 9C). Piper et al. (1999) demonstrate a similar process in the Grand Banks, where a 6^{o} scarp can facilitate debris flow to transform into a supercritical turbidity currents and subsequently start a hydraulic jump. During transportation, though the average slope gradient on the shelf is relatively low (average 0.8^{o}), it is still adequate to support supercritical turbidity currents, as they are above the critical gradient threshold (c. 0.4-0.5^{o}; Fildani et al., 2021). In addition, the hydraulic jumps could strengthen turbulence within the turbidity current (Mulder and Cochonat, 1996), promoting the erosional process and maintaining the steep lee side (Fildani et al., 2006). As the lee side is steep, the hydraulic jumps can be sustained, and the repeated hydraulic jumps may facilitate long runout distances of turbidity currents (Fildani et al., 2006). We infer that this current transformation makes the newly transformed flow competent to establish erosional conditions, leaving variable erosional features on the seabed and becoming sufficiently large and energetic to carry coarse grained sediments to reach the lower slope and even the basin floor. Additionally, this current transformation has unraveled the puzzle for the long-distance transportation ability of the DSWC, since turbidity currents can often extend hundreds of kilometers in submarine setting (i.e. Pirmez and Imran, 2003).

When and where do this transformation occur?

The study area is not the only place where such current transformation occurs, similar diagnostics have been found in the SW Adriatic margin and the NW Mediterranean Seas. In the SW Adriatic margin, where DSWC flows into Gondola Slide's headwall scarp region, the DSWC creates an area of extreme seabed complexity characterised by several large-scale scours aligned in a channel template (cf. Figure 7 of Canals et al., 2009). In the Bari Canyon system, Trincardi et al. (2007) proved that when intense DSWC flows through the canyon head, it can be captured, confined, and transported in a flow regime similar to that of a turbidity current. In the NW Mediterranean Seas, when DSWC cascading into and channelizing through the head of the Cap de Creus

Canyon, it carries coarse particles and forms field of giant furrows and overconsolidated the substrate mud (Puig et al., 2008; Puig, 2017). Additionally, when DSWC cascades into the canyon heads of the Bourcart Canyon, the current accelerates and transports coarser particles than before entering the canyon head (Gaudin et al., 2006). All the seabed geomorphologies and erosive features identified in previous studies require directional, stable and highly energetic processes to develop. Although the published works interpret these erosional features as being formed by the DSWC (Canals et al., 2006; Puig et al., 2008), it is highly reasonable that the DSWC interacted with the pre-existing seabed topographies and transformed into a turbidity current before creating these erosional bedforms. The transformed turbidity current thus carry coarse material and abrade the seabed, induce resuspension and generate erosive bedforms.

Submarine landslides (headwall scarps and internal giant blocks) and canyons (sidewalls and internal irregular terraces) can greatly change the seabed geomorphology and thus the seabed gradient. These local seabed complexity with steep scarps can serve as a key precondition factor for subsequent current transformation. When the DSWC move cross these areas, the pre-existing seabed complexity can disturb or breakup the DSWC and cause turbulence and allow sediment build up resuspension that subsequently ignites turbidity current. The seasonal and recurring DSWC could provide sustained sediment accumulation and subsequent resuspension over a long period of time (normally for a few months), thus providing a stable source of initiation of turbidity currents. As the submarine landslides and canyons are ubiquitous features in almost all continental margins, the transformation of the DSWC into turbidity currents should be a common process with global implications. However, this process has been largely underappreciated by previous studies, due to the lack of high-resolution, multidisciplinary geophysical datasets.

The evolution of seabed geomorphology

Cyclic steps and related supercritical bedforms are recognised as fundamentally important building blocks of seabed geomorphology evolution in many submarine settings (Fildani et al., 2006; Covault et al., 2017; Fildani et al., 2021). In the Gippsland Basin, trains of erosional bedforms have been linked to seabed reworking by supercritical turbidity currents. The cyclic steps can represent morphodynamic signals for submarine channel initiation and are significant to the evolution and maintenance of submarine channels and canyons (i.e. Paull et al., 2010; Fildani et al., 2013). The train of cyclic steps develop on the outer shelf could represent an incipient channel in progress (cf. Figure 7 of Fildani et al., 2013; Fildani et al., 2021). Under the continuous erosion associated with subsequent turbidity currents, these cyclic steps could migrate upslope and focus turbidity currents, gradually coalesce and eventually become a developed channel (Figure 10A, 10B; Fildani et al., 2013). The channel could further evolve laterally and longitudinally, ultimately forming a mature submarine drainage network (i.e. canyon) under the maintenance of sediment capture associated with turbidity currents (Figure 10C). On the slope, the supercritical turbidity currents have resulted in considerable seabed erosion, generating widespread gullies that represent an immature drainage system (Figure 10B; Santangelo et al., 2013). With the continuous downslope transportation of the turbidity currents and other gravity flows (i.e. submarine landslide), the gullies will act as preferential conduits for large-scale sediment transfer and may evolve into canyons (Figure 10C; Santangelo et al., 2013).

Implication

For biodiversity and carbon sequestration

The DSWC often occur in late winter to early spring, at a time synchronous with high biological production levels (i.e. marine phytoplankton bloom), the DSWC can thus efficiently transfer significant quantities of minerals, organic material and oxygen, supplying the functioning of continental shelf ecosystems (Sanchez-Vidal et al., 2008). The transformation from DSWC to turbidity current could act as a fast way of fuelling and renewing nutrients from the shallow marine to the deeper marine environment (i.e. water depth>1000 m). This process could significantly enhance biodiversity in the slope and abyssal environment (Danovaro et al., 2009; Harris, 2014). On the other hand, the cascading current can carry huge amount of organic carbon and store them in the shallow marine (Canals et al., 2006). The subsequent transformation to turbidity current allows the shallowly stored organic carbon travel to deeper marine and thus contribute to submarine carbon sequestration as deeper marine has higher reservoir potential and carbon is less likely to return to the atmosphere. Therefore, the current transformation mechanism presented in this study contributes to the ventilation of intermediate and deep waters in the oceans and has a significant impact on biogeochemical cycles and carbon sequestration.

For natural hazard mitigation

Our results reveal that turbidity currents are one of the dominate sedimentary process in the shelf area of the Gippsland Basin. The emplacement of turbidity currents could break valuable seabed telecommunications cables that carry >95% of global data (Carter et al., 2014) and damage submarine pipelines that may cause potential hydrocarbon leakage hazards (Porcile et al., 2020). In 2022, the Australian Government announced new wind farm construction plans on the Victorian Coast in the Gippsland Basin (the same area as this study; see from Victorian State Government website). Therefore, we suggest that future marine spatial planning and offshore constructions should consider a reasonable band of the buffer zone (e.g. 10-20 km wide; Figure 10C) landward to the landslide headwall scarps located in the central shelf. We also indicate that new geological and geophysical datasets (including sedimentary cores, grabbing or dredging samples, additional 3D seismic reflection data, crewed submersible dives, and Autonomous Underwater Vehicles) need to assess modern seabed conditions (oceanographic and geomorphology), to provide better suggestions for future assessments.

The link between climate change and seabed geomorphology evolution

Previous studies have revealed that DSWC events occur with subdecadal frequency and seawater temperature is the sole driver of such current (Ivanov et al., 2004; Canals et al., 2009; Puig, 2017). The seawater temperature variation may significantly influence the path, frequency and intensity of such a current (Herrmann et al., 2008; Puig, 2017). Published works suggest that future extreme climate perturbations can alter the oceanographic condition, enhance or waken DSWC event over human time scales (i.e. a centennial or longer scale; Canals et al., 2009; Micallef and Mountjoy, 2011). More specifically, climate change can alter ocean heat supply which is projected to cause variations in seawater temperature or salinity (Canals et al., 2009; Gales et al., 2021). The variation of seawater temperature and/or salinity could significantly impact the pathway, frequency and intensity of the dense water cascading currents (Canals et al., 2006). Therefore, the location and frequency of the transformation from DSWC to turbidity currents alter correspondingly. This alternation poses a significant implication for the magnitude of principal seabed erosion processes and impacts seabed geomorphology and sedimentation processes.

In the Gippsland Basin, the impact of climate change on the intensity of the BCC also can be related to its countercurrent - the EAC, which is remarkably sensitive to both short and long-term climate variations. As the BCC and EAC flow in opposite directions on the shelf, a weaker EAC may enhance the BCC to allow the latter to extend beyond northern limit of current study area, while a strong EAC may flow far south and compensate for the influences of the BCC (Oke et al., 2019). We acknowledge that future numerical modelling-based studies are needed to validate our new model for turbidity current initiation and the hypothesis that climate change can dictate the fate of DSWC and could induce variations in near-seabed sedimentary processes via controlling cascading water.

CONCLUSION

Our results elucidate the dense shelf water cascade (DSWC) can interact with pre-existing submarine landslides and subsequently transform into (supercritical) turbidity currents. The newly transformed turbidity currents are an effective seabed sculpting tool and hugely influenced the modern seabed geomorphology and sedimentation process. We suggest that this transformation of DSWC to turbidity current, represent an unappreciated, yet an important trigger for turbidites. This current transformation process has facilitated nearshore water and sediment traveling a long distance (> 80 km) and ultimately descending more than 1000 m down the slope. As the DSWC is a climate sensitive process, future extreme weather can predominately influence the seabed geomorphology, sedimentation process and occurrence of geohazards in the Gippsland Basin and on different continental margins worldwide.

ACKNOWLEDGMENTS

We thank Geoscience Australia for providing seismic reflection, multibeam bathymetry, and grain size data for the Gippsland Basin and Bass Canyon. Seismic reflection, multibeam bathymetry and grain size data are available from the Geoscience Australia Data Portal: https://portal.ga.gov.au/persona/marine. We thank Dr Xingxing Wang, Dr

Wei Li, and Dr Yongpeng Qin for their helpful discussions during the preparation of this paper. The first author thanks the Fundamental Research Funds for the Central Universities, the Natural Science Foundation of Shanghai (under Grant No. 23ZR1467800), the Shanghai Sailing Program (under Grant No. 22YF1450100) and State Key Laboratory of Marine Geology (under Grant No. MGZ202303) for their financial support.

FIGURE CAPTIONS

Figure 1. (A) Occurrence previously documented dense shelf water cascade (DSWC) around the world. Numbers in each area refer to the location: (1) Eastern Chukchi Sea shelf, (2) Beaufort Sea shelf, (3) Foxe Basin, northernmost part of Hudson Bay, (4) SW Greenland margin, (5) Northern gulf of California, (6) North American south-eastern shelf, (7) Great Bahama Bank, (8) East Greenland Shelf and south of Denmark Strait, (9) West Spitsbergen shelf, (10) Bear Island Channel, Barents Sea, (11) hindered in Storfjord, Barents Sea, (12) Skagerrak, eastern flank of the North Sea, (13) Rockall Bank, North Atlantic Ocean, (14) Celtic Sea shelf, North Atlantic Ocean, (15) Gulf of Lion, NW Mediterranean Sea, (16) Gondola slide area, Adriatic Sea shelf, (17) Cape Bari, SE Adriatic Sea shelf, (18) Southern Mediterranean Sea shelf, (19) Aegean Sea shelf, (20) Banc d'Arguin, near Cape Blanc and off the west African coast, (21) Western shelf of Novaya Zemlya, Barents Sea, (22) shelf of Nansen Basin, Arctic Ocean, (23) North-eastern Severnaya Zemlya shelf, Laptev Sea, (24) Northern sea of Okhotsk, north-western Pacific Ocean, (25) Peter the Great Bay, near the Japan Sea continental slope, (26) NW Australia inner shelf, (27) Shark Bay, western Australia, (28) Great Australian Bight, southern Australia, (29) Jervis Bay, southern Australia, (30) Bass Strait, south-eastern Australia, (31) Spencer Gulf, east Australia, (32) The Hikurangi subduction margin, SE of central New Zealand, (33) The western Ross Sea, Antarctic Ocean, (34) The Adélie Coast, East Antarctic sector, Antarctic Ocean, (35) Prydz Bay, East Antarctica, (36) Southern margin of Weddell Sea shelf, (37) Eastern margin of Weddell Sea shelf, (38) The southern Ross Sea, Antarctic Ocean. Note that the blue dots are based on the

DSWC global atlas by Ivanov et al. (2004) and the DSWC recorded around Australian shelves by Mahjabin et al. (2020). The pink dots indicate recently reported (2004–present) cascading phenomena measured by long-term and high-frequency in situ measurements globally, see Appendix 2 for the supporting references. (B) Schematics of the DSWC mechanism showing the formation of intermediate nepheloid layers on the shelf and the downslope turbidity currents. Adapted from Fohrmann et al. (1998).

Figure 2. (A) The regional map of Australia, showing the location of the study area (indicated in a red polygon) and the oceanographic setting. The trajectories of the main oceanic currents are represented by white, blue, and yellow dashed lines. LC, Leeuwin Current; SAC, South Australian Current; ZC, Zeehan Current; BCC, Bass Cascade Current; EAC, East Australian Current. In Gippsland Basin, when the BCC flows through the Bass Strait during winter, it is further fed by the LC, ZC and the wind stress within the Bass Strait, jointly transporting Bass Strait water towards the front (Li et al., 2005; Mitchell et al., 2007b). During summer, though the BCC is less active, strong offshore wind and tidal activities can further reinforce and transport Bass Strait water eastwards (Godfrey et al., 1980). (B) Zoom in view of the Gippsland Basin and the Bass Canyon. Note the north arrow (white) and the yellow box denote the location of the 3D seismic data. The transportation pathway of the BCC is based on data collected from the Conductivity, Temperature, Depth (CTD) sensors adopted during the winter of 1981 by Tomczak (1985). The transportation pathway of the EAC is adopted from Lavering (1994) and Ridgway and Hill (2009). (C) Temperature profile of the Bass Strait showing

the downward temperature anomalies within the continental shelf and slope. (D) Temperature profile (potential temperature) in offshore eastern Australia, showing the depth of the East Australian Current (EAC). The temperature data is from the WOCE (World Ocean Current Experiment) Hydrographic Program (available at https://odv.awi.de/data/ocean). See Figure 2A for locations.

Figure 3. (A) 3D view of seabed multibeam bathymetric map of the offshore Gippsland Basin and Bass Canyon system, showing the main geomorphologic features. (B) Sketch of Figure 3A, showing the key depositional elements, canyons and distinguished regional domains. (C) Shelf-to-slope seismic profile showing the Central shelf and slope regions. See Figure 3B for location.

Figure 4. (A) Seabed structure map generated from the 3D seismic data, showing the seabed morphology in the Central Region. (B) Dip illumination attribute map calculated from the 3D seismic data, showing the detailed sedimentary structures of the Central Region. Note the yellow dots indicate the piston core location. (C) Zoomed-in view of the continental shelf in the Central Region, emphasizing the sediment waves, cyclic steps and channels. See Figure 4B for location.

Figure 5. (A) Seismic dip section cut through the headwall scarp of the landslide. (B) Seismic longitudinal profile along the axis of the cyclic step train. (C) Seismic longitudinal profile cutting through the axis of channel-formed cyclic steps. The

inserted schematic map shows a series of idealized asymmetrical cyclic steps and hypothetical densiometric Froude number (Fr) variability. Within a single bedform, the supercritical flow creates a hydraulic jump (Frd>1) at the base of the lee side and transfers to subcritical flow (Frd<1) at the stoss side. Subsequently, the subcritical flow reaccelerates to supercritical flow again down to the lee side of the next bedform. The schematic map was modified by Cartigny et al. (2011). (D) Seismic longitudinal profile cutting through the axis of channel-formed cyclic steps. (E) Seismic crosssectional profile cutting through the channels; note the stair-shaped erosional characteristics of furrows developed on the channel sidewalls. See Figure 4C for locations.

Figure 6. Zoomed-in view of the continental slope in the Central Region, emphasizing the landslides and gullies. See Figure 4B for location.

Figure 7. (A) Seismic section illustrating gullies' cross-sectional geometries. (B) Seismic dip section cutting along the gully ridge. (C) Seismic dip section cutting along the gully ridge. (D) Seismic dip section cutting within the gully and along its thalweg. See Figure 6 for locations.

Figure 8. (A) Core sketch generated based on piston core report from central region of the Gippsland Basin, showing the cross-section of the Facies-1. (B) Core sketch generated based on piston core report, showing the cross-section of Facies-2. Core locations in Figure 4B. (C) Grain size distribution in the Central area of the Gippsland Basin. The blue arrow indicates the transport direction of the BCC. Figure 9. (A) The 3D

view of the Central Region, showing the seabed morphological structures and major current pathways. (B) Schematic 2D plain view of the Central shelf, illustrating the location of headwall scarps, the pathway of the BCC and its associated supercritical turbidity currents. See Figure 9A for location. (C) Schematic cross-section showing the transformation from BCC to turbidity currents. See text for explanation and Figure 9B for location. (D) Schematic cross-section depicting the combined influence of the Westerly Wind, internal waves, and tide-induced sediment resuspension and turbidity current initiation. See Figure 9A for location.

Figure 10. Schematic of seabed geomorphology evolution processes in the Central Region of the Gippsland Basin. (A) Shelf: the transformation of the Bass Cascading Current (BCC) into turbidity currents; Slope: the generation of scarps caused by wave activities near the upper slope. (B) Shelf: The formation of the sedimentary structures caused turbidity currents; Slope: The initiation of gullies and the formation of the landslides on the upper slope. (C) Shelf: The evolution from cyclic steps into channels and canyons; Slope: landslide initiation near the lower slope. Note that the buffer zone indicates a stable seabed not influenced by the current transformation process or the ignited turbidity current.

REFERENCE

Bouma, A.H.P.H.K.F.P.S., 1962. Sedimentology of some Flysch deposits : a graphic approach to facies interpretation. Elsevier, Amsterdam

Boland, F., 1971. Temperature-salinity anomalies at depths between 200m and 800m in the Tasman sea. Marine and Freshwater Research 22, 55-62.

Marshall, N., Stanley, D., Kelling, G., 1978. Large storm-induced sediment slump reopens an unknown Scripps submarine canyon tributary. Sedimentation in submarine canyons, fans, and trenches: Stroudsburg, Pennsylvania, Hutchinson and Ross, 73-84.

Godfrey, J., Jones, I., Maxwell, G., Scott, B., 1980. On the winter cascade from Bass Strait into the Tasman Sea. Marine and Freshwater Research 31, 275-286.

Bea, R.G., Wright, S.G., Sircar, P., Niedoroda, A.W., 1983. Wave-induced slides in south pass block 70, Mississippi Delta. Journal of Geotechnical Engineering 109, 619-644.

Farre, J.A., McGregor, B.A., Ryan, W.B., Robb, J.M., 1983. Breaching the shelfbreak: passage from youthful to mature phase in submarine canyon evolution.

Flood, R.D., 1983. Classification of sedimentary furrows and a model for furrow initiation and evolution. Geological Society of America Bulletin 94, 630-639.

Tomczak, 1985. The Bass Strait water cascade during winter 1981. Continental Shelf Research 4, 255-278.

Rahmanian, V., Moore, P., Mudge, W., Spring, D., 1990. Sequence stratigraphy and the habitat of hydrocarbons, Gippsland Basin, Australia. Geological Society, London, Special Publications 50, 525-544.

Colwell, J.B., Constantine, A.E., Willcox, J.B., 1993. Regional structure of the Gippsland Basin: interpretation and mapping of a deep seismic data set. Australian Geological Survey Organisation.

Lavering, I.H., 1994. Marine environments of Southeast Australia (Gippsland Shelf and Bass Strait) and the impact of offshore petroleum exploration and production activity. Marine georesources & geotechnology 12, 201-226.

Mulder, T., Cochonat, P., 1996. Classification of offshore mass movements. Journal of Sedimentary research 66, 43-57.

Fohrmann, H., Backhaus, J.O., Blaume, F., Rumohr, J., 1998. Sediments in bottom-arrested gravity plumes: Numerical case studies. Journal of Physical Oceanography 28, 2250-2274.

Hill, P., Exon, N., Keene, J., Smith, S., 1998. The continental margin off east Tasmania and Gippsland: structure and development using new multibeam sonar data. Exploration Geophysics 29, 410-419.

Piper, D.J., Cochonat, P., Morrison, M.L., 1999. The sequence of events around the epicentre of the 1929 Grand Banks earthquake: initiation of debris flows and turbidity current inferred from sidescan sonar. Sedimentology 46, 79-97.

Lee, S., Chough, S., 2001. High‐resolution (2–7 kHz) acoustic and geometric characters of submarine creep deposits in the South Korea Plateau, East Sea. Sedimentology 48, 629-644.

Exon, N., Hill, P., Partridge, A., Chaproniere, G., Keene, J., 2002. Cretaceous volcanogenic and Miocene calcareous strata dredged from the deepwater Gippsland Basin on RV Franklin Research Cruise FR11/98. Geoscience Australia Record 7.

Wynn, R.B., Stow, D.A., 2002. Recognition and interpretation of deep-water sediment waves-implications for palaeoceanography, hydrocarbon exploration and flow process interpretation (Introduction to special issue). Marine Geology 192, 1-3.

Pirmez, C., Imran, J., 2003. Reconstruction of turbidity currents in Amazon Channel. Marine and petroleum geology 20, 823-849.

Ivanov, V., Shapiro, G., Huthnance, J., Aleynik, D., Golovin, P., 2004. Cascades of dense water around the world ocean. Progress in oceanography 60, 47-98.

Li, F., Dyt, C., Griffiths, C., Jenkins, C., Rutherford, M., Chittleborough, J., 2005. Seabed sediment transport and offshore pipeline risks in the Australian southeast. The APPEA Journal 45, 523-534.

Taki, K., Parker, G., 2005. Transportational cyclic steps created by flow over an erodible bed. Part 1. Experiments. Journal of Hydraulic Research 43, 488-501.

Canals, M., Puig, P., de Madron, X.D., Heussner, S., Palanques, A., Fabres, J., 2006. Flushing submarine canyons. Nature 444, 354-357.

Fildani, A., Normark, W.R., Kostic, S., Parker, G., 2006. Channel formation by flow stripping: Large‐scale scour features along the Monterey East Channel and their relation to sediment waves. Sedimentology 53, 1265-1287.

Gaudin, M., Berné, S., Jouanneau, J.-M., Palanques, A., Puig, P., Mulder, T., Cirac, P., Rabineau, M., Imbert, P., 2006. Massive sand beds attributed to deposition by dense water cascades in the Bourcart canyon head, Gulf of Lions (northwestern Mediterranean Sea). Marine Geology 234, 111-128.

Mitchell, J., Holdgate, G., Wallace, M., 2007a. Pliocene–Pleistocene history of the Gippsland Basin outer shelf and canyon heads, southeast Australia. Australian Journal of Earth Sciences 54, 49-64.

Mitchell, J., Holdgate, G., Wallace, M., Gallagher, S., 2007b. Marine geology of the Quaternary Bass Canyon system, southeast Australia: a cool-water carbonate system. Marine geology 237, 71-96.

Trincardi, F., Foglini, F., Verdicchio, G., Asioli, A., Correggiari, A., Minisini, D., Piva, A., Remia, A., Ridente, D., Taviani, M., 2007. The impact of cascading currents on the Bari Canyon System, SW-Adriatic margin (Central Mediterranean). Marine Geology 246, 208-230.

Herrmann, M., Estournel, C., Déqué, M., Marsaleix, P., Sevault, F., Somot, S., 2008. Dense water formation in the Gulf of Lions shelf: Impact of atmospheric interannual variability and climate change. Continental Shelf Research 28, 2092-2112.

Ogston, A.S., Drexler, T.M., Puig, P., 2008. Sediment delivery, resuspension, and transport in two contrasting canyon environments in the southwest Gulf of Lions. Continental Shelf Research 28, 2000-2016.

Puig, P., Palanques, A., Orange, D., Lastras, G., Canals, M., 2008. Dense shelf water cascades and sedimentary furrow formation in the Cap de Creus Canyon, northwestern Mediterranean Sea. Continental Shelf Research 28, 2017-2030.

Sanchez‐Vidal, A., Pasqual, C., Kerhervé, P., Calafat, A., Heussner, S., Palanques, A., Durrieu de Madron, X., Canals, M., Puig, P., 2008. Impact of dense shelf water cascading on the transfer of organic matter to the deep western Mediterranean basin. Geophysical Research Letters 35.

Bull, S., Cartwright, J., Huuse, M., 2009. A subsurface evacuation model for submarine slope failure. Basin Research 21, 433-443.

Canals, M., Danovaro, R., Heussner, S., Lykousis, V., Puig, P., Trincardi, F., Calafat, A.M., de

Madron, X.D., Palanques, A., Sanchez-Vidal, A., 2009. Cascades in Mediterranean submarine grand canyons. Oceanography 22, 26-43.

Danovaro, R., Canals, M., Gambi, C., Heussner, S., Lampadariou, N., Vanreusel, A., 2009. Exploring benthic biodiversity patterns and hotspots on European margin slopes. Oceanography 22, 16-25.

Noormets, R., Dowdeswell, J., Larter, R.D., Cofaigh, C.Ó., Evans, J., 2009. Morphology of the upper continental slope in the Bellingshausen and Amundsen Seas–Implications for sedimentary processes at the shelf edge of West Antarctica. Marine Geology 258, 100-114.

Piper, D.J., Normark, W.R., 2009. Processes that initiate turbidity currents and their influence on turbidites: a marine geology perspective. Journal of Sedimentary Research 79, 347-362.

Ridgway, K., Hill, K., 2009. The East Australian Current.

James, N.P., Bone, Y., 2010. Neritic carbonate sediments in a temperate realm: southern Australia. Springer Science & Business Media.

Paull, C.K., Ussler III, W., Caress, D.W., Lundsten, E., Covault, J.A., Maier, K.L., Xu, J., Augenstein, S., 2010. Origins of large crescent-shaped bedforms within the axial channel of Monterey Canyon, offshore California. Geology 6, 755-774.

Vetter, E.W., Smith, C.R., De Leo, F.C., 2010. Hawaiian hotspots: enhanced megafaunal abundance and diversity in submarine canyons on the oceanic islands of Hawaii. Marine Ecology 31, 183-199.

Cartigny, M.J., Postma, G., Van den Berg, J.H., Mastbergen, D.R., 2011. A comparative study of sediment waves and cyclic steps based on geometries, internal structures and numerical modeling. Marine Geology 280, 40-56.

Kostic, S., 2011. Modeling of submarine cyclic steps: Controls on their formation, migration, and architecture. Geosphere 7, 294-304.

Micallef, A., Mountjoy, J.J., 2011. A topographic signature of a hydrodynamic origin for submarine gullies. Geology 39, 115-118.

Gales, J., Larter, R., Mitchell, N., Hillenbrand, C.D., Østerhus, S., Shoosmith, D., 2012. Southern Weddell Sea shelf edge geomorphology: Implications for gully formation by the overflow of high‐salinity water. Journal of Geophysical Research: Earth Surface 117.

Fildani, A., Hubbard, S.M., Covault, J.A., Maier, K.L., Romans, B.W., Traer, M., Rowland, J.C., 2013. Erosion at inception of deep-sea channels. Marine and Petroleum Geology 41, 48-61.

Lonergan, L., Jamin, N.H., Jackson, C.A.-L., Johnson, H.D., 2013. U-shaped slope gully systems and sediment waves on the passive margin of Gabon (West Africa). Marine Geology 337, 80-97.

Santangelo, M., Gioia, D., Cardinali, M., Guzzetti, F., Schiattarella, M., 2013. Interplay between mass movement and fluvial network organization: An example from southern Apennines, Italy. Geomorphology 188, 54-67.

Talling, P.J., Paull, C.K., Piper, D.J., 2013. How are subaqueous sediment density flows triggered, what is their internal structure and how does it evolve? Direct observations from monitoring of active flows. Earth-Science Reviews 125, 244-287.

Carter, L., Gavey, R., Talling, P.J., Liu, J.T., 2014. Insights into submarine geohazards from breaks in subsea telecommunication cables. Oceanography 27, 58-67.

Cetina‐Heredia, P., Roughan, M., Van Sebille, E., Coleman, M., 2014. Long‐term trends in the East Australian Current separation latitude and eddy driven transport. Journal of Geophysical

Research: Oceans 119, 4351-4366.
Harris, P.T., 2014. Shelf and deep-sea sedimentary environments and physical benthic disturbance regimes: a review and synthesis. Marine Geology 353, 169-184.
Moors-Murphy, H.B., 2014. Submarine canyons as important habitat for cetaceans, with special reference to the Gully: a review. Deep Sea Research Part II: Topical Studies in Oceanography 104, 6-19.
Postma, G., Cartigny, M.J., 2014. Supercritical and subcritical turbidity currents and their deposits—A synthesis. Geology 42, 987-990.
Talling, P.J., 2014. On the triggers, resulting flow types and frequencies of subaqueous sediment density flows in different settings. Marine Geology 352, 155-182.
Zhong, G., Cartigny, M.J., Kuang, Z., Wang, L., 2015. Cyclic steps along the South Taiwan Shoal and West Penghu submarine canyons on the northeastern continental slope of the South China Sea. Bulletin 127, 804-824.
Hebbeln, D., Van Rooij, D., Wienberg, C., 2016. Good neighbours shaped by vigorous currents: Cold-water coral mounds and contourites in the North Atlantic. Marine Geology 378, 171-185.
Covault, J.A., Kostic, S., Paull, C.K., Sylvester, Z., Fildani, A., 2017. Cyclic steps and related supercritical bedforms: building blocks of deep-water depositional systems, western North America. Marine Geology 393, 4-20.
Pittock, A.B., 2017. Climate change: turning up the heat. Routledge.
Puig, P., 2017. Dense shelf water cascading and associated bedforms, Atlas of bedforms in the western mediterranean. Springer, pp. 35-40.
Amblas, D., Dowdeswell, J., 2018. Physiographic influences on dense shelf-water cascading down the Antarctic continental slope. Earth-Science Reviews 185, 887-900.
O'Brien, P., Mitchell, C., Nguyen, D., Langford, R., 2018. Mass Transport Complexes on a Cenozoic paleo-shelf edge, Gippsland basin, southeastern Australia. Marine and Petroleum Geology 98, 783-801.
Oke, P.R., Roughan, M., Cetina-Heredia, P., Pilo, G.S., Ridgway, K.R., Rykova, T., Archer, M.R., Coleman, R.C., Kerry, C.G., Rocha, C., 2019. Revisiting the circulation of the East Australian Current: Its path, separation, and eddy field. Progress in Oceanography 176, 102139.
Mahjabin, T., Pattiaratchi, C., Hetzel, Y., 2020. Occurrence and seasonal variability of Dense Shelf Water Cascades along Australian continental shelves. Scientific reports 10, 1-13.
Morrison, A., Hogg, A.M., England, M.H., Spence, P., 2020. Warm Circumpolar Deep Water transport toward Antarctica driven by local dense water export in canyons. Science advances 6, eaav2516.
Porcile, G., Bolla Pittaluga, M., Frascati, A., Sequeiros, O.E., 2020. Typhoon-induced megarips as triggers of turbidity currents offshore tropical river deltas. Communications Earth & Environment 1, 1-13.
Slootman, A., Cartigny, M.J., 2020. Cyclic steps: Review and aggradation-based classification. Earth-Science Reviews 201, 102949.
Fildani, A., Kostic, S., Covault, J.A., Maier, K.L., Caress, D.W., Paull, C.K., 2021. Exploring a new breadth of cyclic steps on distal submarine fans. Sedimentology 68, 1378-1399.
Gales, J., Rebesco, M., De Santis, L., Bergamasco, A., Colleoni, F., Kim, S., Accettella, D., Kovacevic, V., Liu, Y., Olivo, E., 2021. Role of dense shelf water in the development of Antarctic submarine canyon morphology. Geomorphology 372, 107453.

Wu, N., Nugraha, H.D., Zhong, F.G., Steventon, M., 2021. The role of mass-transport complexes (MTCs) in the initiation and evolution of submarine canyons.

Post, A.L., Przeslawski, R., Nanson, R., Siwabessy, J., Smith, D., Kirkendale, L.A., Wilson, N.G., 2022. Modern dynamics, morphology and habitats of slope-confined canyons on the northwest Australian margin. Marine Geology 443, 106694.

Figure 1

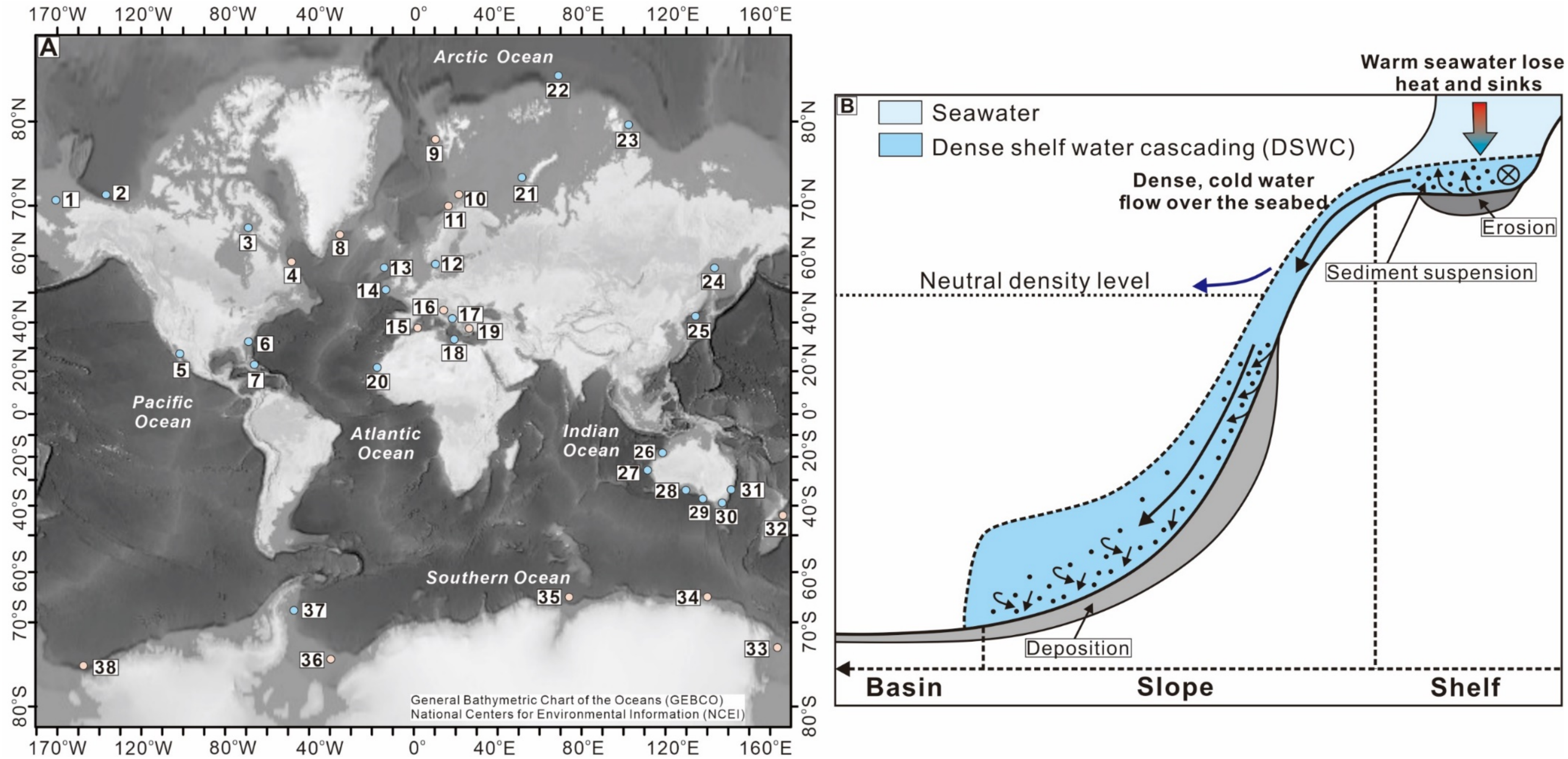

A
Arctic Ocean
Pacific Ocean
Atlantic Ocean
Indian Ocean
Southern Ocean
General Bathymetric Chart of the Oceans (GEBCO)
National Centers for Environmental Information (NCEI)
B
Seawater
Dense shelf water cascading (DSWC)
Warm seawater lose heat and sinks
Dense, cold water flow over the seabed
Erosion
Sediment suspension
Neutral density level
Deposition
Basin
Slope
Shelf

Figure 2

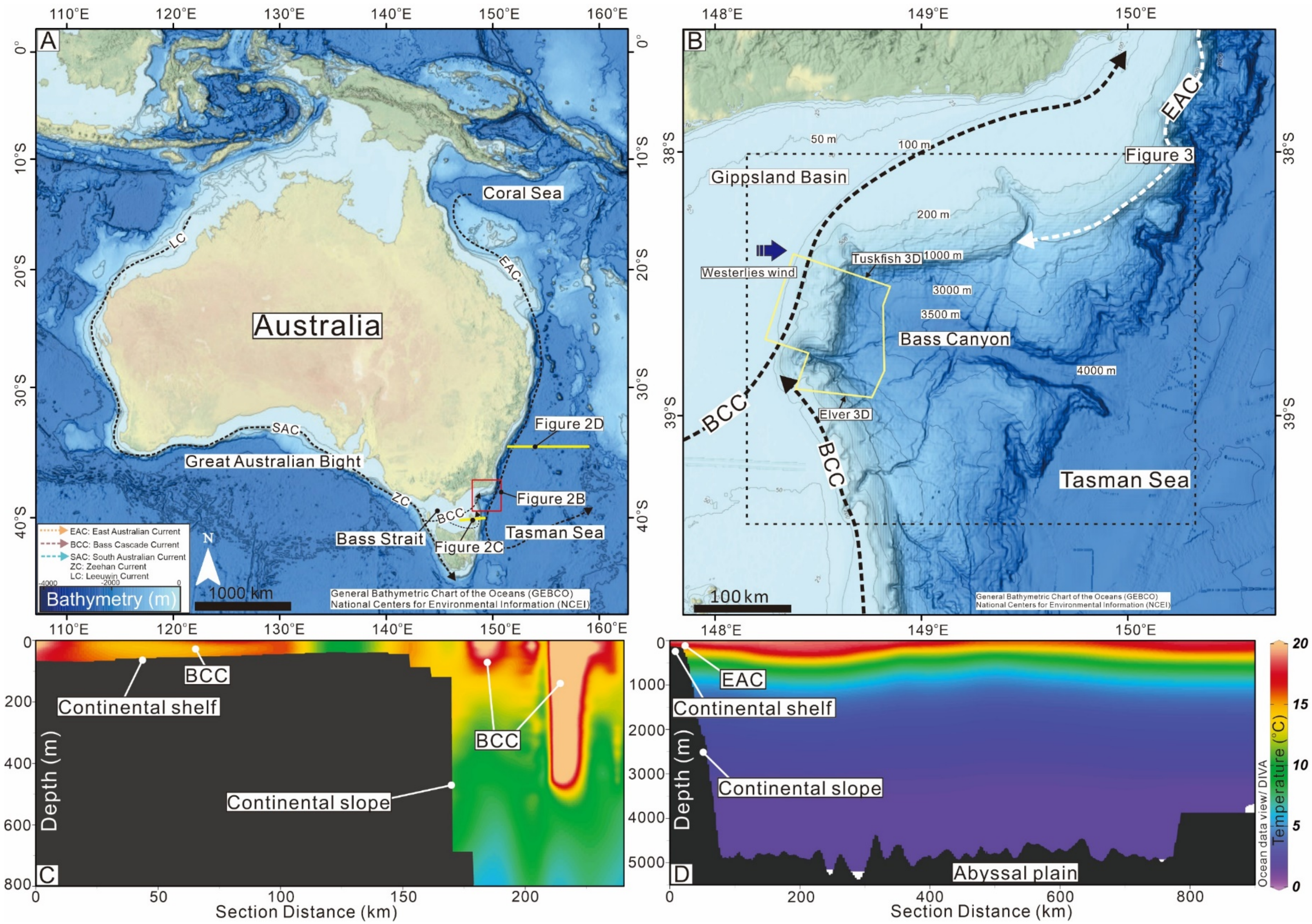

A
B
C
D
Australia
Coral Sea
LC
EAC
SAC
ZC
BCC
Great Australian Bight
Bass Strait
Tasman Sea
Figure 2B
Figure 2C
Figure 2D
EAC: East Australian Current
BCC: Bass Cascade Current
SAC: South Australian Current
ZC: Zeehan Current
LC: Leeuwin Current
Bathymetry (m)
1000 km
General Bathymetric Chart of the Oceans (GEBCO)
National Centers for Environmental Information (NCEI)
Gippsland Basin
Figure 3
Westerlies wind
Tuskfish 3D
Elver 3D
Bass Canyon
50 m
100 m
200 m
1000 m
3000 m
3500 m
4000 m
100 km
Continental shelf
Continental slope
Abyssal plain
Depth (m)
Section Distance (km)
Temperature (°C)
Ocean data view/ DIVA

Figure 3

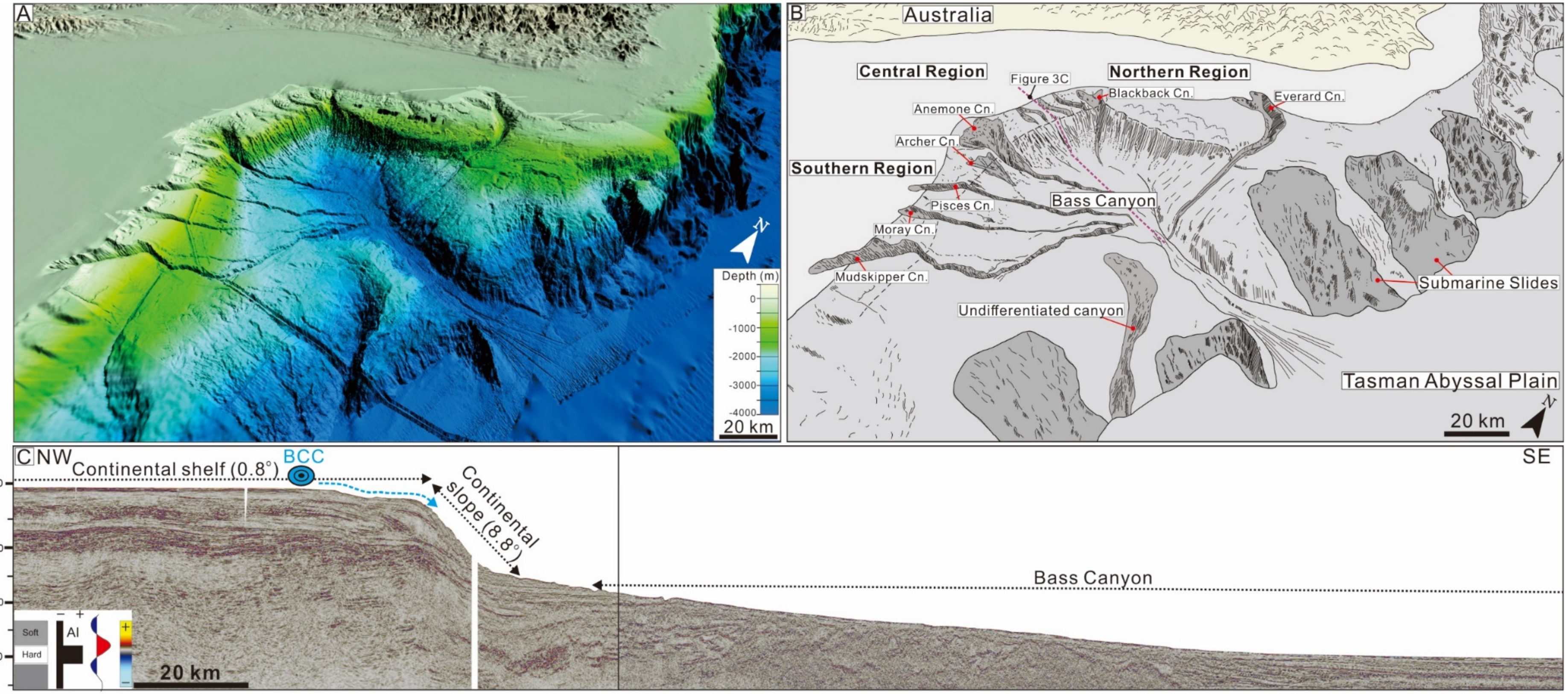
A
Depth (m)
0
-1000
-2000
-3000
-4000
20 km
N
B
Australia
Central Region
Northern Region
Figure 3C
Blackback Cn.
Everard Cn.
Anemone Cn.
Archer Cn.
Southern Region
Pisces Cn.
Bass Canyon
Moray Cn.
Mudskipper Cn.
Submarine Slides
Undifferentiated canyon
Tasman Abyssal Plain
20 km
N
C
NW
Continental shelf (0.8°)
BCC
Continental slope (8.8°)
SE
TWT (ms)
0
-2000
-4000
-6000
Bass Canyon
Soft
Hard
AI
20 km

Figure 4

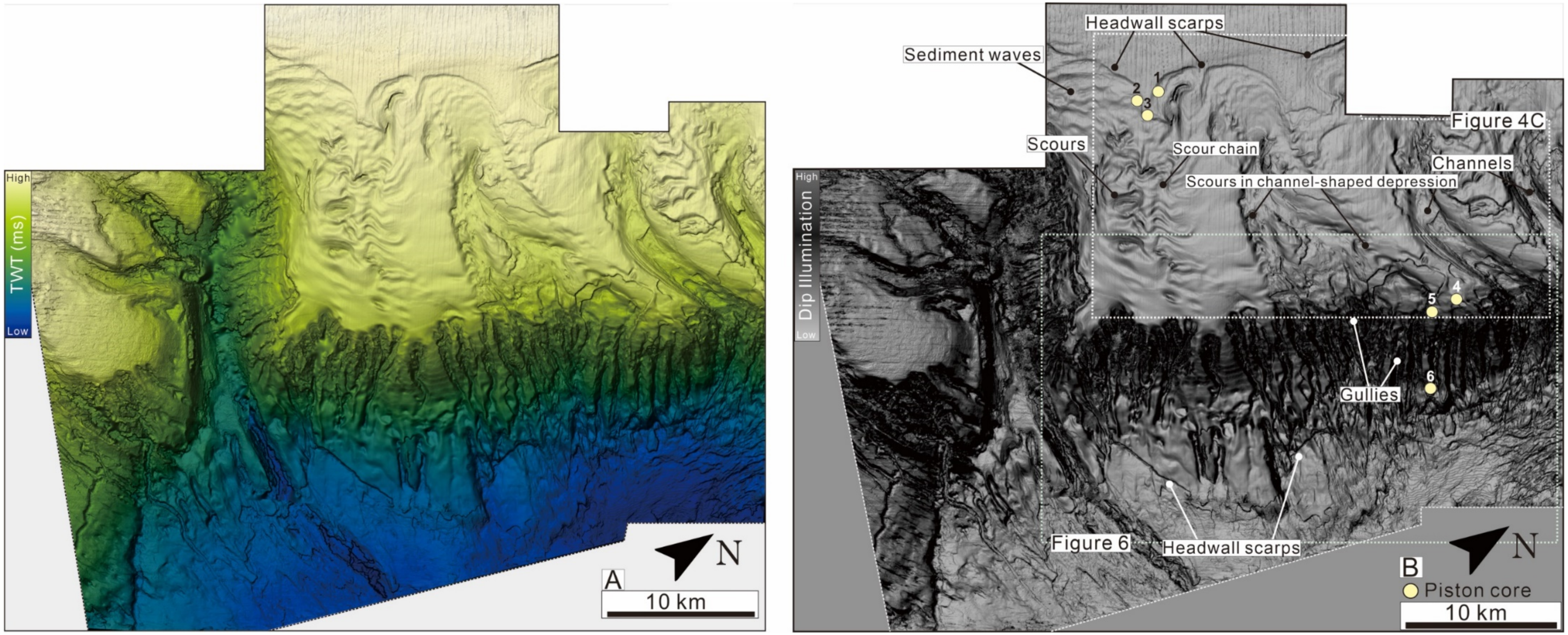
High
TWT (ms)
Low
A
N
10 km
Headwall scarps
Sediment waves
1
2
3
Figure 4C
Scours
Scour chain
Channels
Scours in channel-shaped depression
High
Dip Illumination
Low
5
4
6
Gullies
Figure 6
Headwall scarps
N
B
Piston core
10 km

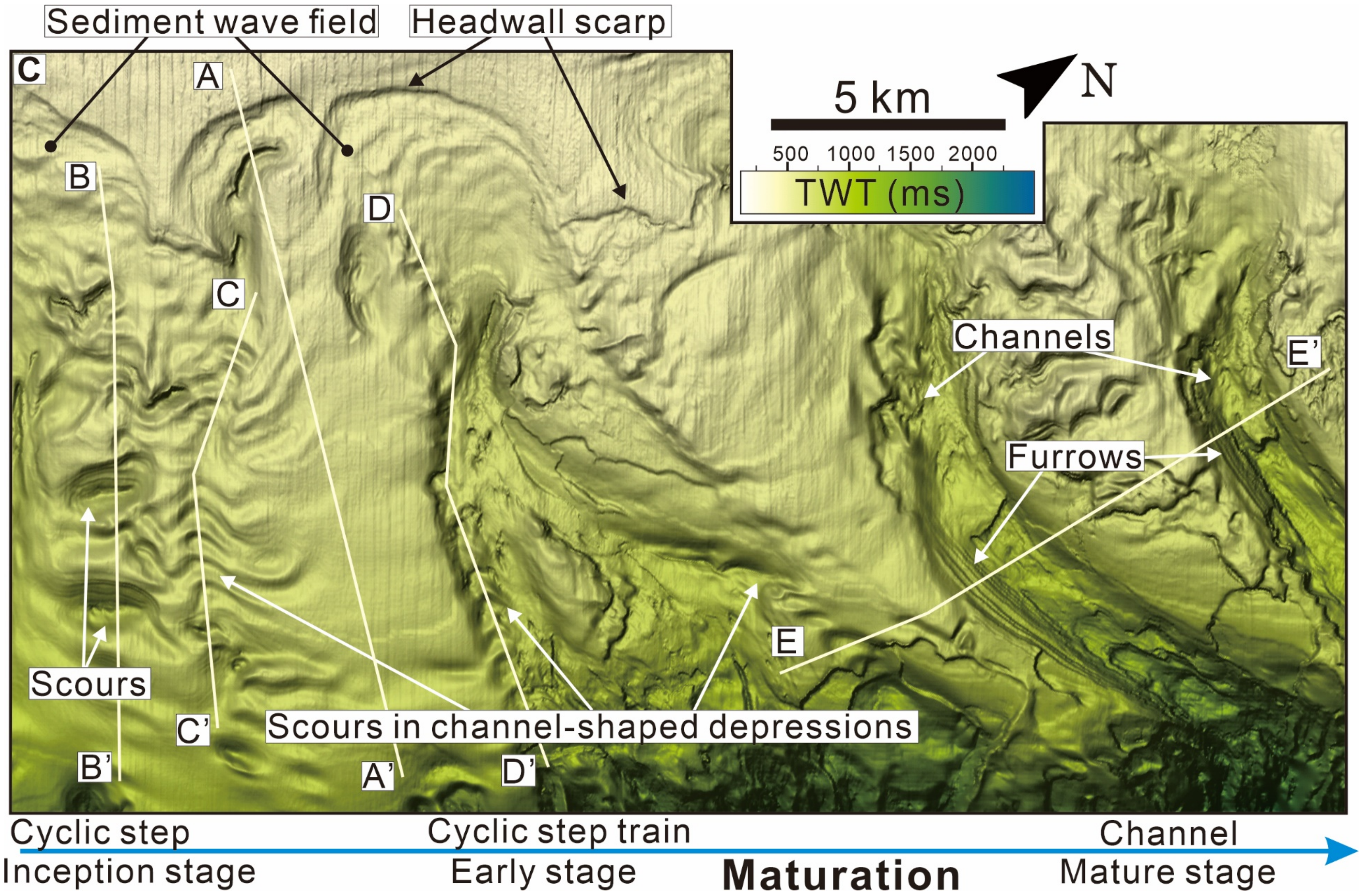
Sediment wave field
Headwall scarp
C
A
B
D
C
5 km
N
500 1000 1500 2000
TWT (ms)
Channels
E'
Furrows
E
Scours
C'
Scours in channel-shaped depressions
B'
A'
D'
Cyclic step
Inception stage
Cyclic step train
Early stage
Maturation
Channel
Mature stage

Figure 5

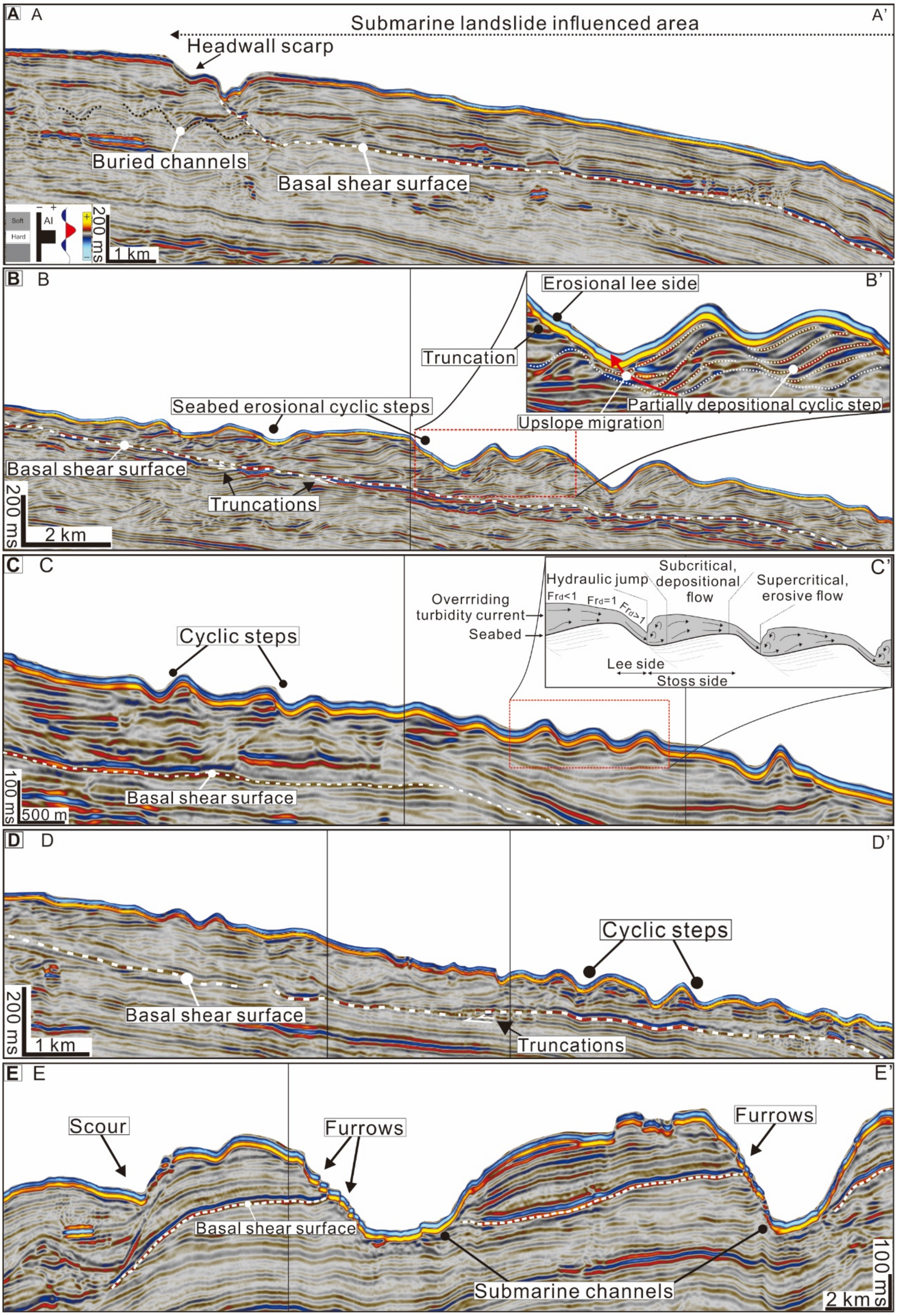

A A A'
Submarine landslide influenced area
Headwall scarp
Buried channels
Basal shear surface
Soft
Hard
AI
200 ms
1 km
B B B'
Erosional lee side
Truncation
Partially depositional cyclic step
Upslope migration
Seabed erosional cyclic steps
Basal shear surface
Truncations
200 ms
2 km
C C C'
Hydraulic jump
Subcritical, depositional flow
Supercritical, erosive flow
Overrriding turbidity current
Seabed
Lee side
Stoss side
Cyclic steps
Basal shear surface
100 ms
500 m
D D D'
Cyclic steps
Basal shear surface
Truncations
200 ms
1 km
E E E'
Scour
Furrows
Furrows
Basal shear surface
Submarine channels
100 ms
2 km

Figure 6

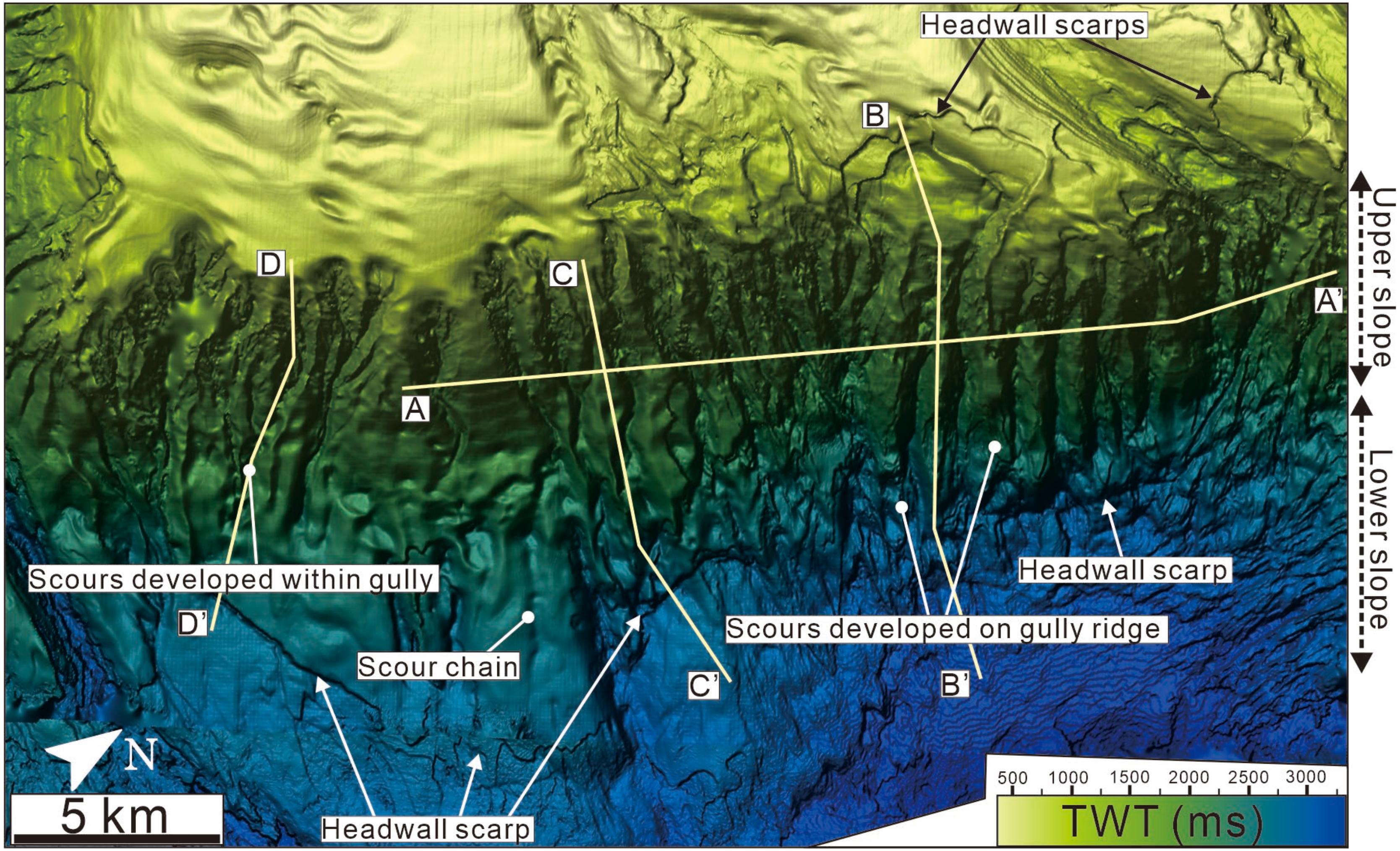
Headwall scarps
B
D
C
A'
A
Upper slope
Lower slope
Scours developed within gully
D'
Scour chain
Headwall scarp
C'
Scours developed on gully ridge
B'
N
5 km
Headwall scarp
500 1000 1500 2000 2500 3000
TWT (ms)

Figure 7

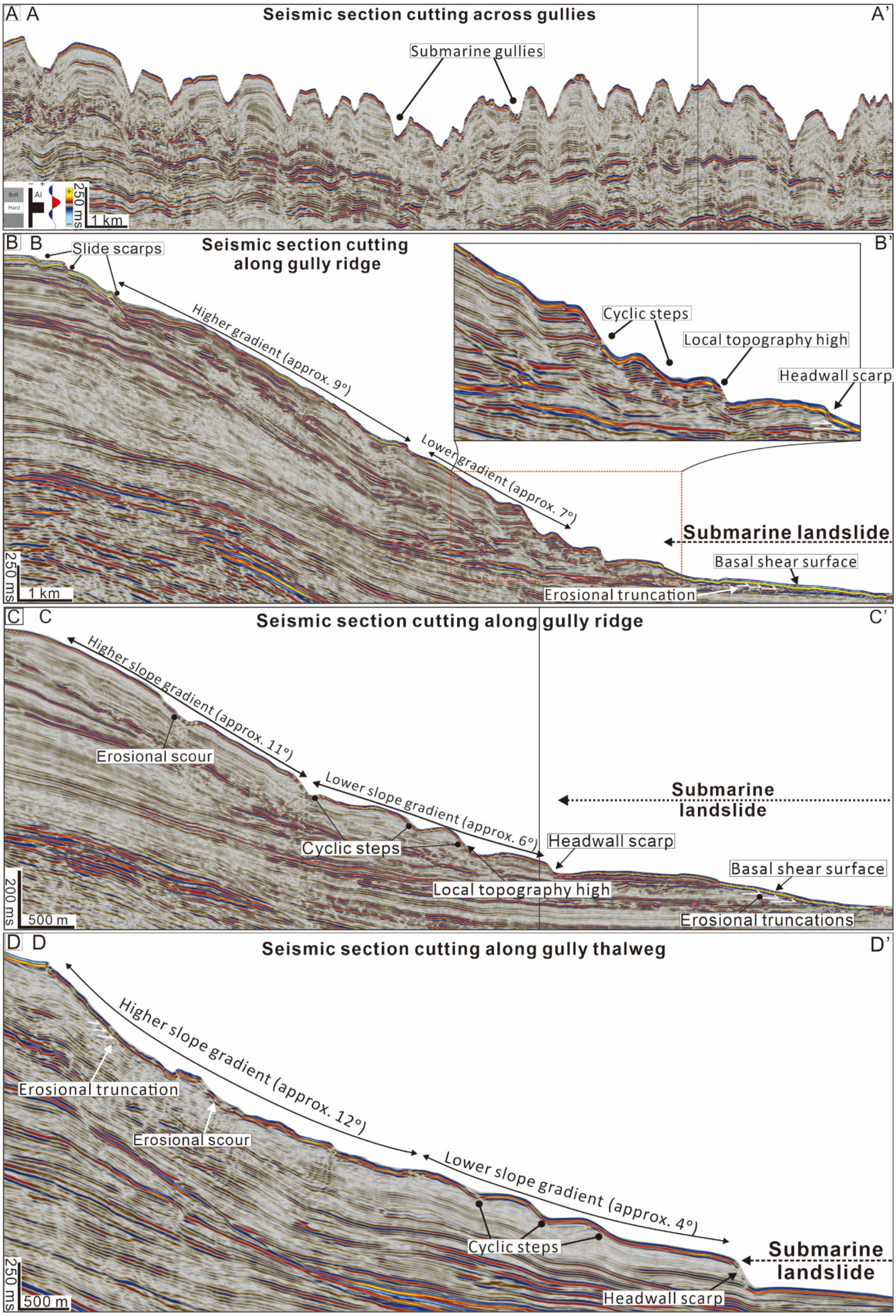

A A
Seismic section cutting across gullies
A'
Submarine gullies
Soft
Hard
AI
250 ms
1 km
B B
Slide scarps
Seismic section cutting along gully ridge
B'
Higher gradient (approx. 9°)
Lower gradient (approx. 7°)
Cyclic steps
Local topography high
Headwall scarp
Submarine landslide
Basal shear surface
Erosional truncation
250 ms
1 km
C C
Seismic section cutting along gully ridge
C'
Higher slope gradient (approx. 11°)
Erosional scour
Lower slope gradient (approx. 6°)
Cyclic steps
Headwall scarp
Submarine landslide
Local topography high
Basal shear surface
Erosional truncations
200 ms
500 m
D D
Seismic section cutting along gully thalweg
D'
Higher slope gradient (approx. 12°)
Erosional truncation
Erosional scour
Lower slope gradient (approx. 4°)
Cyclic steps
Submarine landslide
Headwall scarp
250 ms
500 m

Figure 8

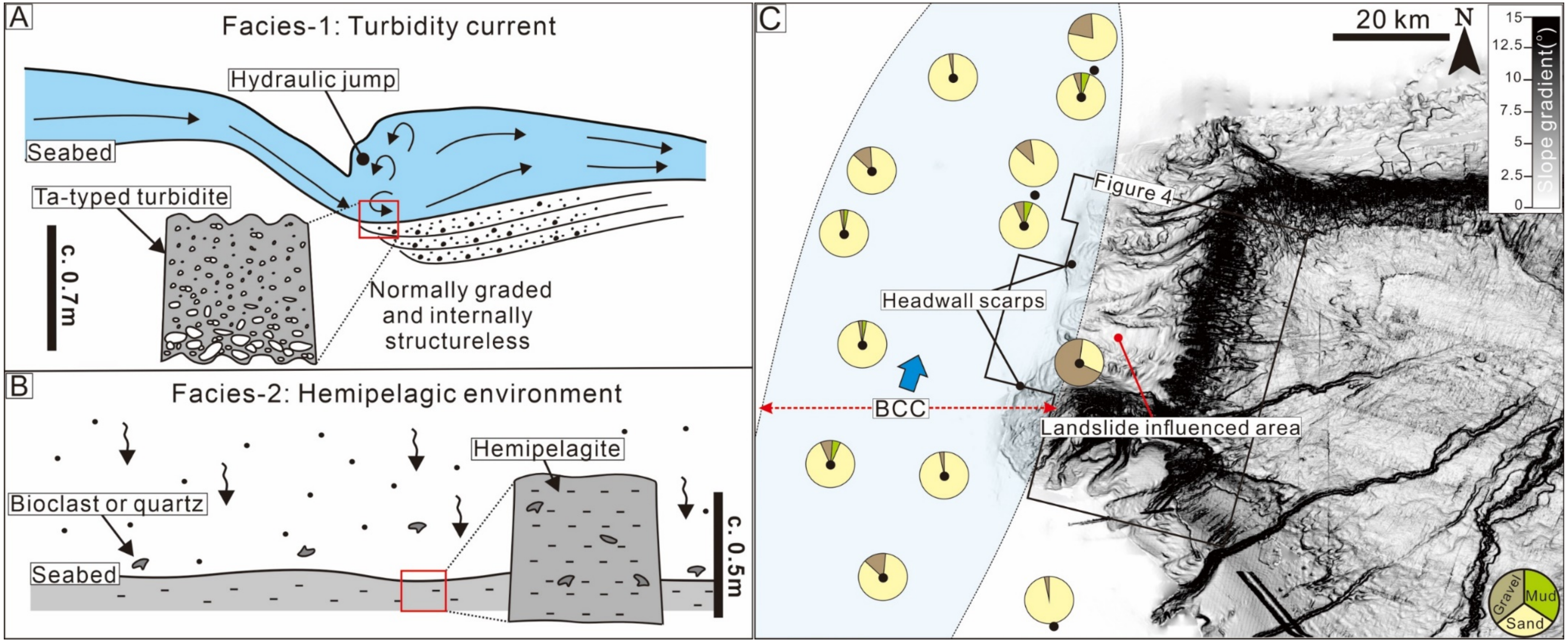
A
Facies-1: Turbidity current
Hydraulic jump
Seabed
Ta-typed turbidite
c. 0.7m
Normally graded
and internally
structureless
B
Facies-2: Hemipelagic environment
Hemipelagite
Bioclast or quartz
Seabed
c. 0.5m
C
20 km
N
15
12.5
10
7.5
5
2.5
0
Slope gradient(°)
Figure 4
Headwall scarps
BCC
Landslide influenced area
Gravel
Mud
Sand

Figure 9

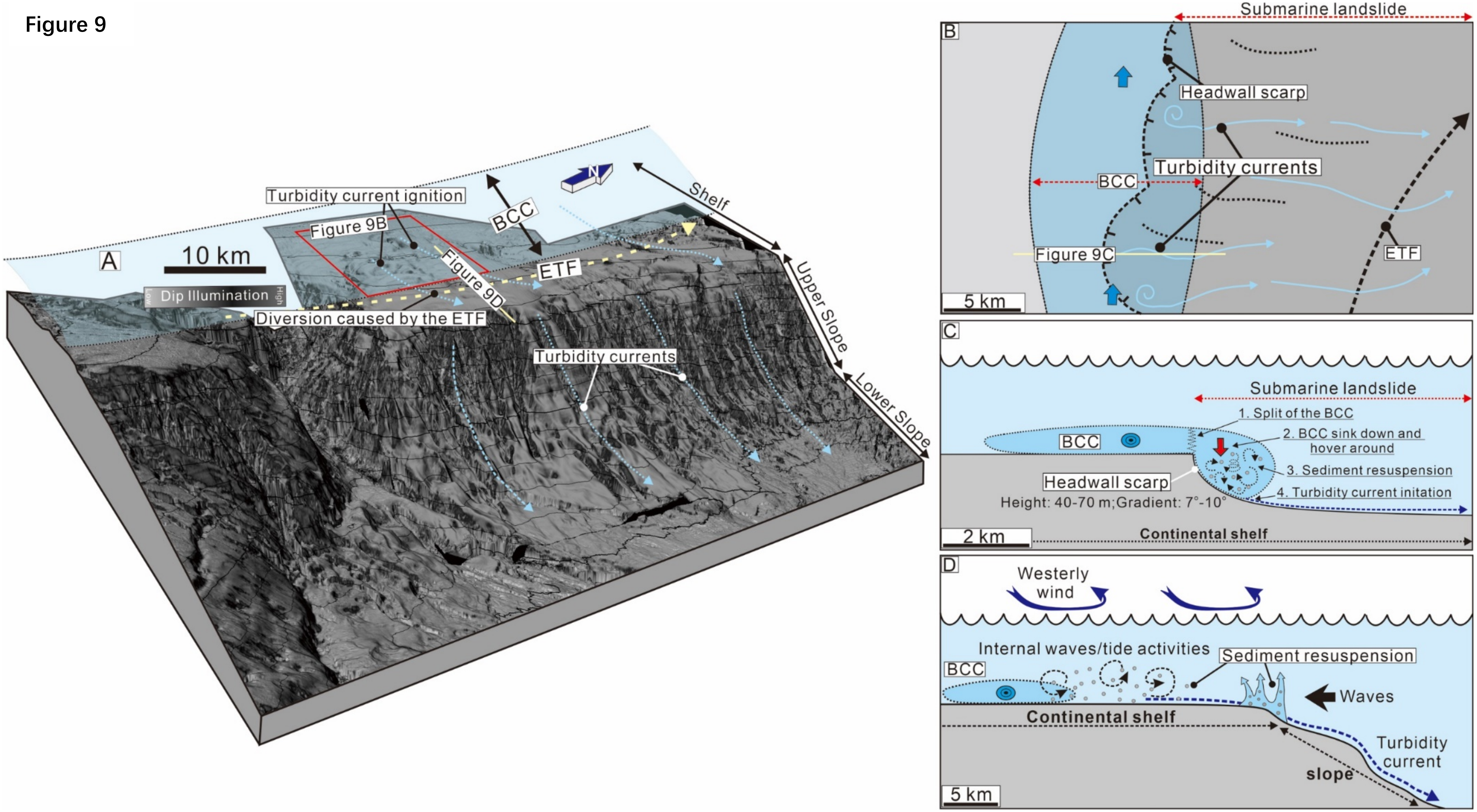

A
10 km
Dip Illumination
Low
High
Turbidity current ignition
Figure 9B
Figure 9D
BCC
ETF
N
Shelf
Upper Slope
Lower Slope
Diversion caused by the ETF
Turbidity currents
B
Submarine landslide
Headwall scarp
Turbidity currents
BCC
Figure 9C
ETF
5 km
C
Submarine landslide
1. Split of the BCC
2. BCC sink down and hover around
3. Sediment resuspension
4. Turbidity current initation
BCC
Headwall scarp
Height: 40-70 m;Gradient: 7°-10°
2 km
Continental shelf
D
Westerly wind
Internal waves/tide activities
Sediment resuspension
BCC
Waves
Continental shelf
Turbidity current
slope
5 km

Figure 10

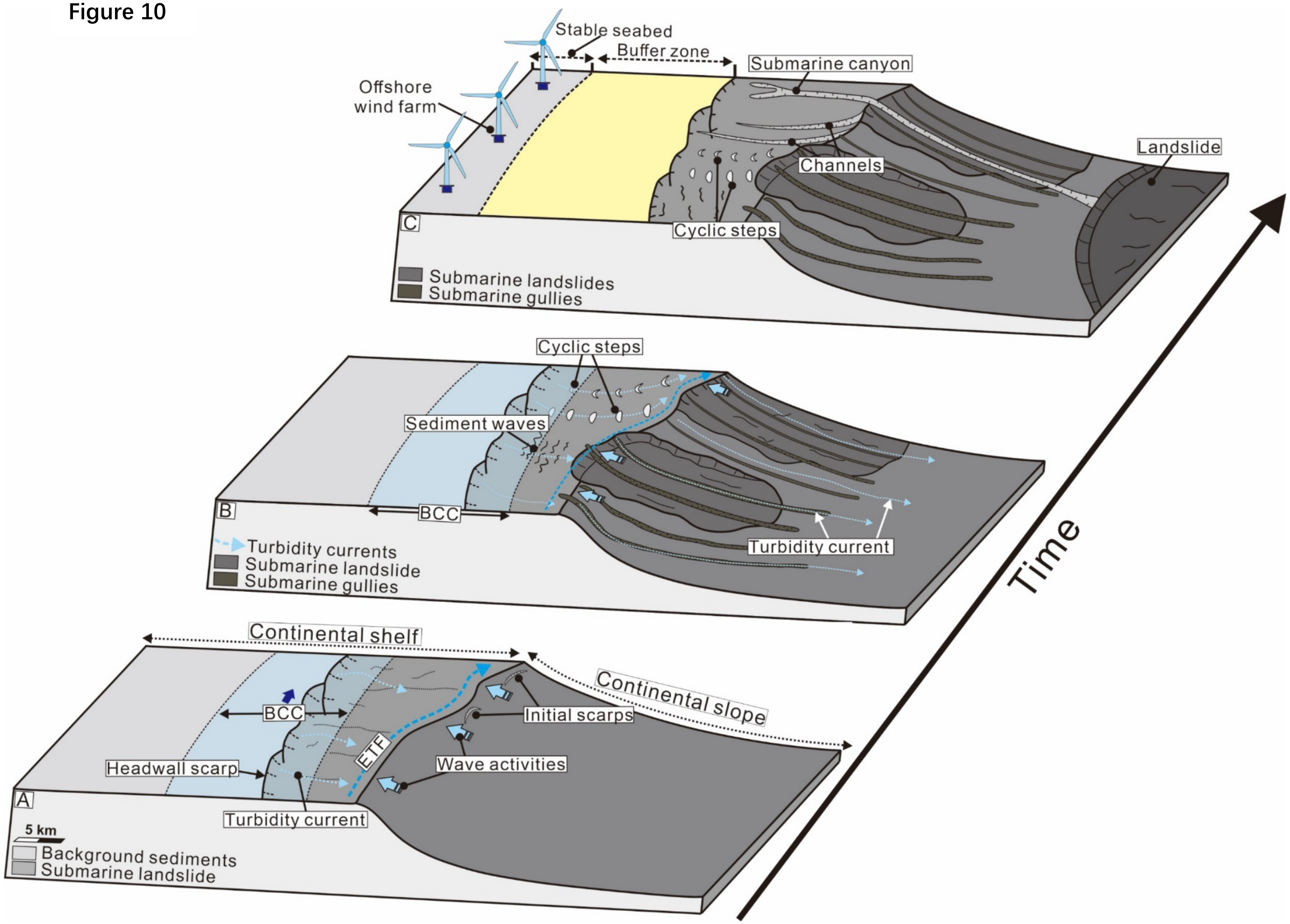

Stable seabed
Buffer zone
Submarine canyon
Offshore wind farm
Landslide
Channels
Cyclic steps
C
Submarine landslides
Submarine gullies
Cyclic steps
Sediment waves
BCC
B
Turbidity current
Turbidity currents
Submarine landslide
Submarine gullies
Time
Continental shelf
Continental slope
BCC
Initial scarps
ETF
Wave activities
Headwall scarp
A
Turbidity current
5 km
Background sediments
Submarine landslide